

Low-field Classroom Nuclear Magnetic Resonance System

by

Clarissa Lynette Zimmerman

Submitted to the Department of Electrical Engineering and Computer Science

in partial fulfillment of the requirements for the degree of

Master of Engineering in Electrical Engineering and Computer Science

at the

MASSACHUSETTS INSTITUTE OF TECHNOLOGY

February 2010

© Massachusetts Institute of Technology 2010. All rights reserved.

Author
Department of Electrical Engineering and Computer Science
February 4, 2010

Certified by
Edward S. Boyden
Assistant Professor
Thesis Supervisor

Accepted by
Arthur C. Smith
Chairman, Department Committee on Graduate Theses

Low-field Classroom Nuclear Magnetic Resonance System

by

Clarissa Lynette Zimmerman

Submitted to the Department of Electrical Engineering and Computer Science
on February 4, 2010, in partial fulfillment of the
requirements for the degree of
Master of Engineering in Electrical Engineering and Computer Science

Abstract

The goal of this research was to develop a Low-field Classroom NMR system that will enable hands-on learning of NMR and MRI concepts in a Biological-Engineering laboratory course.

A permanent magnet system, designed using finite-element modeling software, was built to produce a static field of $\vec{B}_0 = 0.133$ Tesla. A single coil was used for both transmitting the excitation pulses and detecting the NMR signal. The probe circuit is essentially an LC tank with a tunable resonant frequency. An FPGA is used to produce the excitation pulses and process the received NMR signals.

This research has led to the ability to observe Nuclear Magnetic Resonance. ‘Spin-Lattice’ and ‘Spin-Spin’ relaxation times of glycerin samples can easily be measured. Future work will allow further MRI exploration by incorporating gradient magnetic field coils.

Thesis Supervisor: Edward S. Boyden

Title: Assistant Professor

Contents

1	Introduction	13
1.1	Motivation	13
1.2	Background	14
1.2.1	NMR overview	14
1.2.2	Relaxation	18
1.2.3	Imaging	23
1.3	Past Work	25
2	Pulse Generation and Signal Conditioning Design	29
2.1	Design 1	29
2.1.1	Transmit Chain	29
2.1.2	Receive Chain	31
2.1.3	Isolation	34
2.2	Design 2	36
2.2.1	Transmit Chain	36
2.2.2	Receive Chain	37
2.2.3	Isolation	38
3	Magnetic Circuit Design and Assembly	39
3.1	Preliminary Magnetic System	42
3.1.1	Preliminary Magnetic Design Assembly	43
3.2	Improved Magnetic System	44
3.2.1	Improved Magnetic Design Assembly	45

3.3	Magnetic Design Comparison	47
4	Probe Design	49
4.1	Transmit/Receive Coil Background	49
4.2	Coil Design	52
4.3	Probe Circuit Design	55
5	Results	61
5.1	Experimental Implementation	61
5.1.1	System assembly	61
5.1.2	Implementing Experiment	65
5.2	Results	67
5.2.1	Mapping Tip Angle to Pulse Widths	68
5.2.2	Pulse Sequence Scope Shots	69
5.2.3	Time Constant Measurement	70
6	Conclusion	75
A	Software	79
A.1	LabVIEW pulse generator	79
A.2	FPGA Verilog code	80
A.2.1	top level	80
A.2.2	Configuration Registers	91
A.2.3	Signal Gate	93
A.2.4	Window Function Generator	95
A.2.5	Sinewave Generator	96
A.2.6	Frequency Multiplier	98
A.2.7	FIR Filter	99
B	Magnetic Design Drawings	105

List of Figures

1-1	Classical picture of a hydrogen nucleus in the static field, \vec{B}_0	15
1-2	The precessional motion of the the atomic nuclei's magnetic moment is equivalent to the motion of a spinning top [9].	15
1-3	NMR precession and relaxation	16
1-4	Relaxation of \vec{M} components.	17
1-5	Free Inductance Decay Curve	18
1-6	Diagram of the inversion recovery sequence.	19
1-7	M_z recovery curve ($180^\circ - 90^\circ$ pulse sequence).	20
1-8	M_z recovery curve ($90^\circ - 90^\circ$ pulse sequence).	21
1-9	M_{xy} decay curve.	21
1-10	Spin-echo diagram.	23
1-11	Spin-echo signal [8].	23
1-12	Figure of past work in [10]	25
1-13	Figure of past work in [4]	26
1-14	Block diagram of the 'Junior Lab' pulsed NMR system at MIT	27
2-1	Block diagram of the two system designs (without and with the FPGA)	29
2-2	Transmit chain in System Design 1 (no FPGA).	30
2-3	LabVIEW front panel of the Pulse Generator program	30
2-4	Receive chain in System Design 1 (no FPGA).	32
2-5	Simple passive low-pass filter used to filter high frequency residue from the modulated NMR signal.	33

2-6	The transmit and receive signal chains are isolated with crossed diode pairs.	35
2-7	Transmit chain in System Design 2 (with FPGA).	37
2-8	Receive chain in System Design 2 (with FPGA).	37
3-1	Quickfield simulations of a variety of magnetic circuit geometries. The figures show a color map of the flux density and magnetic field lines. .	41
3-2	Preliminary Magnetic System Design	42
3-3	Improved Magnetic System Design	45
3-4	Comparison of simulated field in the preliminary magnet and improved magnet designs.	47
4-1	Demonstration of Ampere’s Law in a solenoid.	50
4-2	Demonstration of Faraday’s law in a loop of wire.	51
4-3	Photo of a coil being made.	54
4-4	A series LC tank circuit, including the intrinsic resistance of the inductor.	55
4-5	Schematic of the resonant circuit with tuning and matching capacitors.	56
4-6	Preliminary magnetic system probe circuit simulation	58
4-7	Improved magnetic system probe circuit simulation	59
5-1	PCB layout the probe circuit	61
5-2	Photos of probe holder assembly.	63
5-3	Photo of the electronic components box.	64
5-4	Photo of the ‘power supply board’.	64
5-5	Experimental setup for finding an initial NMR signal.	67
5-6	Series of oscilloscope photos that show the effect of frequency mixing the NMR signal.	67
5-7	Close-up shots of received FID curve and echo signal.	68
5-8	Preliminary magnetic system pulse width measurement.	68
5-9	Improved magnetic system pulse width measurement.	69
5-10	Oscilloscope shots of pulse sequences.	70

5-11	T_2^* plot	71
5-12	Preliminary magnetic system T_2 data.	72
5-13	Improved magnetic system T_2 data.	73
5-14	Preliminary magnetic system T_1 data.	73
5-15	Improved magnetic system T_1 data.	74
A-1	LabVIEW block diagram of the pulse generation program.	79
B-1	Solidworks drawing of the low-carbon steel yoke and cylindrical spacers used in the improved magnetic system.	106
B-2	Solidworks drawing of the machined pole pieces used in the improved magnetic system.	107

List of Tables

1.1	Relaxation Time Constants Summary	24
4.1	Coil 1 Properties	54
4.2	Coil 2 Properties	55
4.3	Calculated tuning and matching capacitor values.	56

Chapter 1

Introduction

1.1 Motivation

The goal of this research was to develop a low-field classroom nuclear magnetic resonance system (NMR). The primary motivation for this research was the need for students to understand the principles of NMR which is the basis for its medical imaging application, MRI.

The popularity of Magnetic Resonance Imaging (MRI) compared to other medical imaging methods is due to two things: its safety and flexibility. As a diagnostic and research tool, MRI is considered safe because it is non-invasive and does not use ionizing radiation. As a relatively new imaging technique, there is an abundance of active research in the field of MRI, which continues to contribute to the already broad range of MRI functionality. Some of the diverse uses of MRI include: a variety of imaging contrasts for anatomical imaging, blood flow imaging, diffusion imaging, and brain activation mapping (functional MRI). [5]

NMR is the response of nuclear magnetic moments to external magnetic fields. While NMR is the basis of MRI technology, it is also the basis of other technologies such as NMR spectroscopy which is used for chemical analysis. Because of the ubiquity of NMR as the basic principle behind MRI and other technologies, it is an important topic of learning for science and engineering students, particularly in bio-engineering.

The current NMR system presented here achieves pulsed NMR capabilities and can implement various pulse sequences and measurements. The system will be used in an MIT laboratory course, Biological Instrumentation and Measurement. Further work may extend the system presented here for MRI.

The Biological Instrumentation and Measurement course, 20.309, consists of hands-on learning of essential concepts in instrumentation. The students learn about fundamental concepts in optics, electronics, and frequency domain analysis. They then apply those concepts in the lab by building their own instruments, in some cases, or experimenting with ‘home-made’ instruments which are transparent in functionality. The addition of the NMR system to the course will enable the understanding of one of the most important diagnostic and scientific tools today, MRI. Nuclear Magnetic Resonance concepts are typically difficult for students to grasp; the classroom system should assist with this issue.

1.2 Background

NMR technology is based on the relationship between the magnetic moments of atomic nuclei and external magnetic fields and the ability to observe that interaction. NMR physics has roots in quantum mechanics, however, there is also a classical picture of NMR which is commonly used.

A brief overview of NMR concepts is presented as background. The system is currently intended for pulse NMR experiments and imaging involving hydrogen atoms. Therefore, spectroscopy and chemical shift concepts are not covered.

1.2.1 NMR overview

The hydrogen nucleus has an intrinsic angular momentum, which can be referred to as the nuclear spin. The angular momentum leads to a rotating charge, or tiny current loop, which generates a magnetic moment [8]. \vec{M} is defined as the average magnetic dipole density and is referred to as the magnetization of the sample. At thermal equilibrium, in the presence of a large static field, \vec{B}_0 , \vec{M} aligns with \vec{B}_0 (this

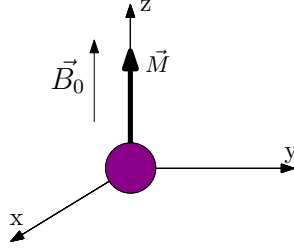


Figure 1-1: Classical picture of a hydrogen nucleus in the static field, \vec{B}_0 .

is the lowest energy orientation). This situation is shown in figure 1-1. When \vec{M} is perturbed from alignment with \vec{B}_0 , it exhibits precessional motion about the axis of \vec{B}_0 , which is generally is the \hat{z} direction. Precession is the same motion that a spinning top exhibits when it starts to fall out of vertical alignment (figure 1-2).

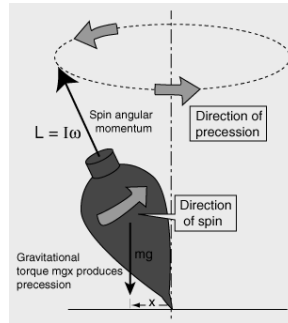


Figure 1-2: The precessional motion of the the atomic nuclei's magnetic moment is equivalent to the motion of a spinning top [9].

The precession of \vec{M} is modeled in figure 1-3. If we do not consider relaxation (a process that will be described later), the motion of \vec{M} is described as

$$\frac{d\vec{M}}{dt} = \gamma \vec{M} \times \vec{B}_0. \quad (1.1)$$

γ is the 'gyromagnetic ratio', a constant that is specific to the type of atomic nuclei.

An important property of the precession is its frequency. The frequency of precession, ω_o , is linearly dependent on the strength of \vec{B}_0 and is known as the Larmor frequency. The angle of \vec{M} from \hat{z} does not affect this frequency. The expression for the Larmor frequency is

$$\omega_o = \gamma B_0, \quad \text{where} \quad (1.2)$$

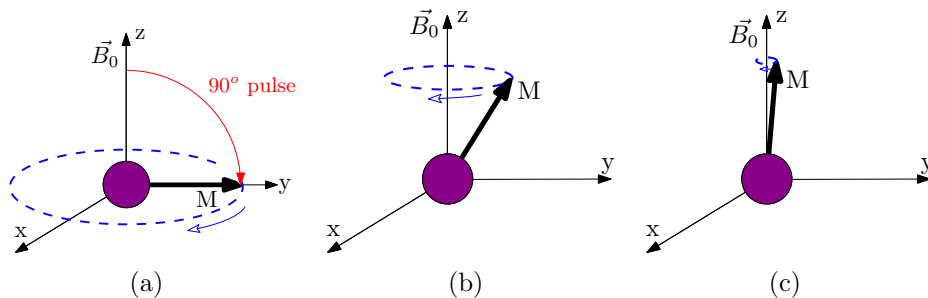


Figure 1-3: Demonstration that precession is most obvious directly after a 90° pulse, and that precession becomes less obvious as the M_{xy} component of \vec{M} decreases.

$$\gamma = 42.576 \text{ MHz/T} \quad \text{for Hydrogen.} \quad (1.3)$$

The magnetization vector, \vec{M} , can be decomposed into a transverse component, M_{xy} , and a longitudinal component, M_z . Without considering relaxation, the equations of motion for these components are

$$\frac{dM_z}{dt} = 0 \quad \text{and} \quad (1.4)$$

$$\frac{dM_{xy}}{dt} = \gamma M_{xy} \times \vec{B}_0. [8] \quad (1.5)$$

At thermal equilibrium, \vec{M} is aligned with \vec{B}_0 . Therefore, ($M_z = M_{eq}$, $M_{xy} = 0$), and precession is not visible. However when another magnetic field that is orthogonal to \vec{B}_0 perturbs \vec{M} from equilibrium, M_{xy} is non-zero and precession can be observed. Precession is most obvious when the \vec{M} is perturbed 90 degrees from \vec{B}_0 as in fig. 1-3(a). After the magnetization is perturbed from equilibrium, it begins to realign with \vec{B}_0 while it is precessing. This process is called relaxation and results in a loss of observed signal (figure 1-3(b) and 1-3(c)). While, figure 1-3 shows this process with \vec{M} , figure 1-4 shows this process with the transverse and longitudinal components of \vec{M} .

NMR experiments can be thought of as having two stages: excitation and acquisition. The critical components of NMR are:

1. A large static homogeneous magnetic field (\vec{B}_0)
2. A coil to generate the resonant (and typically RF) excitation field (\vec{B}_1), which

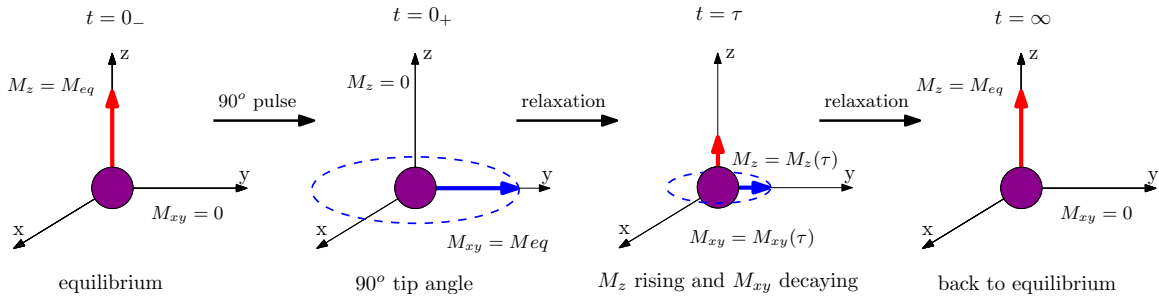


Figure 1-4: Relaxation of \vec{M} components.

is perpendicular to \vec{B}_0 .

3. A coil used to measure the precession of the spins. This may be the same coil that was used to generate the excitation field, \vec{B}_1 .
4. A sample that has the ‘spin’ property

During the excitation stage, the nuclear spins are perturbed from alignment with the static field, \vec{B}_0 . This is done by applying a magnetic pulse at the Larmor frequency, \vec{B}_1 , with the transmit coil. Typical Larmor frequencies are in the RF range so \vec{B}_1 is often called the RF field. The word “resonance” in NMR corresponds to the necessity of matching the excitation field frequency with the frequency of nuclear precession. When \vec{B}_1 is at the Larmor frequency and applied perpendicular to \vec{B}_0 , it rotates \vec{M} . The amount by \vec{M} is rotated is referred to as the tip angle, θ , which depends on the duration and amplitude of the RF pulse. This process can be seen as an energy transfer. At equilibrium, \vec{M} is aligned with \vec{B}_0 , which is the lowest energy state. When energy is transferred with the RF pulse, the magnetization vector \vec{M} is perturbed.

The second stage of pulsed NMR involves observing the precession of the nuclear spins. The orientation of \vec{M} can be measured by the interaction of the magnetization with a “receive coil”. Although the magnetic moment of each spin is infinitesimal, a significant magnetization can be measured from the sum of the magnetic moments in a small volume. From Faraday’s law, we know that a changing magnetic field in a coil (produced by the precessing magnetic moments) induces an electromotive force (emf). This corresponds to a voltage that may be measured and recorded.

The amplitude of the voltage generated across the coil corresponds to the magnitude of the transverse component of the magnetization vector, M_{xy} . It is essential to understand that only the transverse component of \vec{M} can be directly measured. This is because precession is a rotational motion in the transverse plane (which is shown in figures 1-3 and 1-4). This means that the maximum NMR signal is observed when M_{xy} is maximized, which is when the tip angle is 90° . The precession is measured by orienting the receive coil in the transverse plane (perpendicular to \vec{B}_0). In pulsed NMR, the time-domain NMR signal that is transduced with the receive coil is either a free-inductance decay (FID) curve or an echo. An FID curve is shown in figure 1-5.

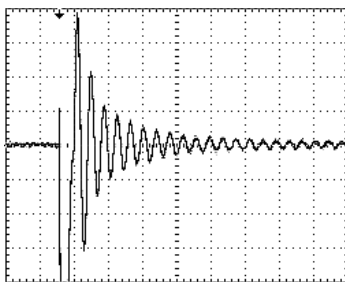


Figure 1-5: Free Inductance Decay Curve (FID).

1.2.2 Relaxation

After \vec{M} is rotated onto the transverse plane, the observed signal decays as \vec{M} begins to re-align with \vec{B}_0 . This process is called relaxation, and is a result of proton interactions and proton interaction with the lattice. For simplicity, let's think of these relaxations occurring after a 90° pulse is applied to the sample in thermal equilibrium. After the 90° pulse the magnetization vector, \vec{M} , is completely in the x-y plane, with no z component. This is shown figure 1-4. The return to equilibrium and loss of observed signal are simultaneous. After the pulse, the transverse component decreases to zero, and the longitudinal component increases from 0 to M_{eq} , the magnetization magnitude at thermal equilibrium. It is intuitive to think that these two things are complementary and have the same time constant. However, the proton interactions lead to the addition of different decay parameters to (1.4) and (1.5). According to [8], "The difference is related to the fact that, in contrast to a given magnetic moment,

the magnitude of the macroscopic magnetization is not fixed, since it is the vector sum of (many) proton spins. The components of \vec{M} parallel and perpendicular to the external field ‘relax’ differently in the approach to their equilibrium values.” Table 1.1 summarizes information about the time constants.

Longitudinal Relaxation

The lowest potential energy orientation of the magnetic moments is in alignment with \vec{B}_0 , i.e. in the \hat{z} direction. During the excitation pulse, energy is transferred to the magnetic moments, causing them to re-orient. However, the magnetic moments ‘want’ to be in the position of lowest energy, so the energy is transferred to the lattice through vibration as \vec{M} recovers to its equilibrium orientation. The recovery of the M_z component to M_{eq} is an exponential rise with time constant T_1 . The return to equilibrium is referred to as, T_1 relaxation, longitudinal relaxation, or spin-lattice relaxation.

Measuring M_z and T_1 is not straightforward. This is because, as mentioned earlier, it is only possible to measure the transverse component of the magnetization vector, M_{xy} , because precession in the x-y plane generates the observed NMR signal. However, there are ways to get around this. The most important idea is the following: a 90° pulse rotates the current M_z magnitude onto the transverse plane. So, if a pulse is applied at $t = \tau$, $M_z(\tau)$ is rotated to the transverse plane, and the subsequent FID amplitude is $M_{xy} = M_z(\tau)$. This is the fundamental idea of the inversion recovery process.

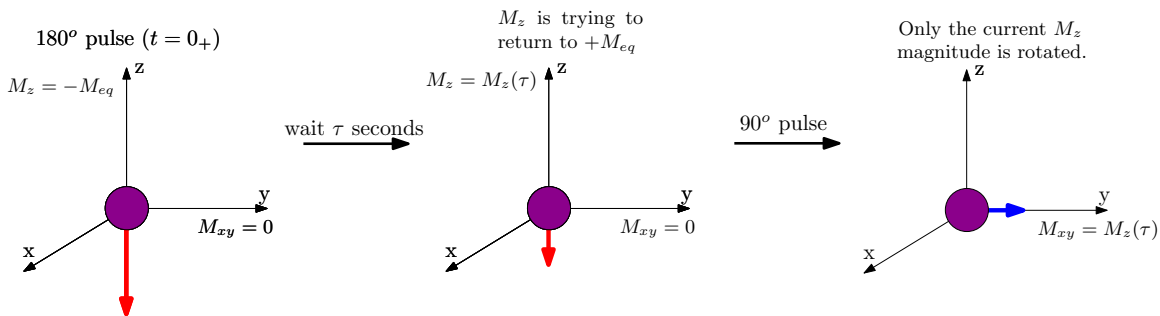


Figure 1-6: Diagram of the inversion recovery sequence.

The inversion recovery sequence proceeds as follows and is illustrated in fig. 1-6:

1. We begin at thermal equilibrium, and then a 180 degree pulse is applied. This rotates $M_z = M_{eq}$ to the $-\hat{z}$ direction.
2. We wait time τ . During this time M_z begins to return to the $+\hat{z}$ direction. So the magnitude of M_z starts as $-M_{eq}$, then eventually passes through zero to return to $+M_{eq}$. After time τ , M_z has made some progress in its return to $+M_{eq}$.
3. A 90° pulse is applied. This rotates $M_z(\tau)$ to the x-y plane.
4. An FID curve is observed. This FID curve has an amplitude that corresponds to $M_z(\tau)$. We can vary τ and measure the amplitude of the FID curve to quantify T_1 relaxation. The data will be of the form: $M_z = M_{eq} - 2M_{eq}e^{-t/T_1}$ as shown in figure 1-7.

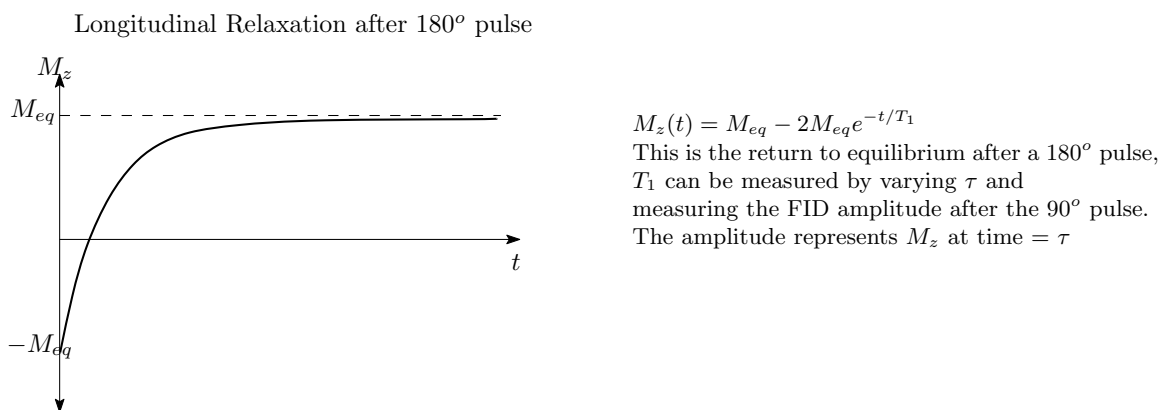


Figure 1-7: M_z recovery curve (180° – 90° pulse sequence).

The inversion recovery sequence is a 180° pulse followed by a 90° pulse. Longitudinal relaxation can also be measured by a 90° – 90° pulse sequence. This is very similar to the 180° – 90° pulse sequence, except that M_z begins the relaxation process at $M_z = 0$ instead of $M_z = -M_{eq}$. So the data would be of the form: $M_z = M_{eq} - M_{eq}e^{-t/T_1}$, as shown in figure 1-8.

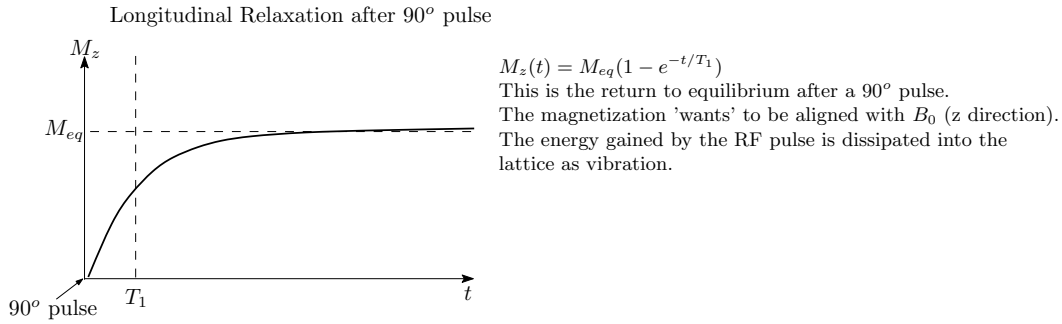


Figure 1-8: M_z recovery curve ($90^\circ - 90^\circ$ pulse sequence).

Transverse relaxation

Transverse relaxation is the exponential decay of M_{xy} with time constant T_2 during the return of \vec{M} to equilibrium. The transverse decay generally proceeds faster than the longitudinal recovery. This is because in addition to energy being transferred to the lattice, the interaction of the magnetic moments of the spins causes M_{xy} to decay faster (this is why transverse relaxation is also known as spin-spin relaxation). This non-reversible decay is shown in figure 1-9.

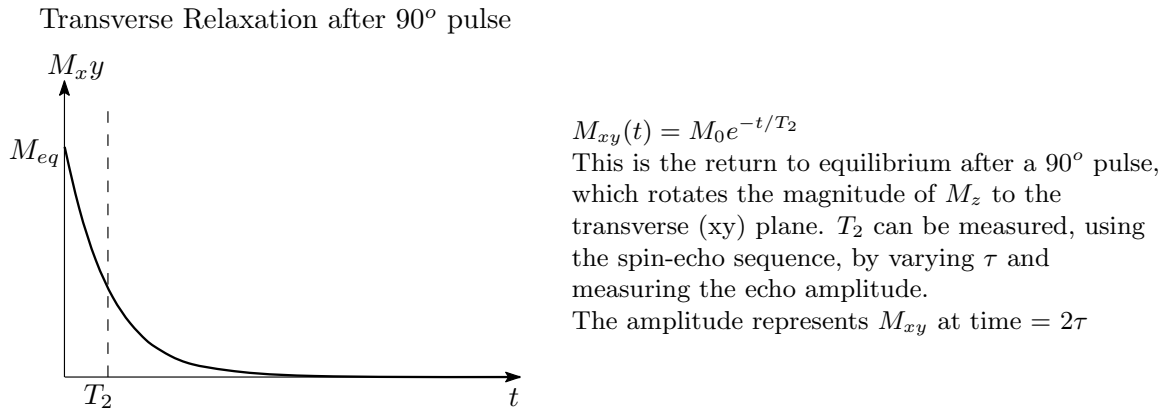


Figure 1-9: M_{xy} decay curve.

There is an additional decay of the observed M_{xy} because of \vec{B}_0 inhomogeneity. The observable transverse magnetization is the FID curve (fig. 1-5), which is the vector sum of the transverse components of the magnetic moments of the sample. This may decay to zero much faster than the actual transverse magnetization of the individual spins. The additional rate of the decay is due to loss of phase-coherence from \vec{B}_0 inhomogeneity. If the field is not homogeneous, which means the field strength or

direction differs slightly over the sample, the frequency at which the spins precess varies slightly. It can be assumed that immediately after the 90° pulse the spins are in phase. However, the varying speed of precession causes them to quickly lose phase coherence (shown in fig. 1-10). As the spins become out of phase, the vector sum of the magnetic moments exponentially diminishes with time constant T_2^* . However, this described 'dephasing' is reversible through the 'spin-echo' pulse sequence. This means that we can reverse the effects of \vec{B}_0 inhomogeneity in order to accurately measure M_{xy} and the the time constant T_2 .

The spin echo sequence proceeds as follows and is illustrated in figures 1-10 and 1-11:

1. A 90° pulse is applied. This causes the magnetization to be rotated into the x-y plane, so $M_{xy} = M_0$ and $M_z = 0$.
2. We wait time τ . During this time we observe the FID curve. This is the signal measured by the coil directly after the 90° pulse. The FID curve exponentially decays with time constant: T_2^* . This decay is due to spin dephasing because of varying precession speeds. A common analogy to use here is a race. By time τ , the runners are spread out due to variation of there speed, and the magnitude of \vec{M} is zero.
3. A 180 degree pulse is applied. This flips the spins across the transverse plane. In the race analogy, the faster runners are now the furthest behind. They are spread out the same way but in reverse. Now as the runners continue, they begin to converge again.
4. We wait time τ again. At time 2τ the runners are completely in phase again. This is the middle of the echo signal shown in figure 1-11. The amplitude of the echo corresponds to $M_0 e^{-2\tau/T_2}$. We can vary τ and use the amplitude of the echo to observe the actual M_{xy} decay. The decay of M_{xy} will be in the form: $M_{xy}(t) = M_0 e^{-t/T_2}$ as shown in figure 1-9.

Table 1.1 summarizes the relaxation time constant properties.

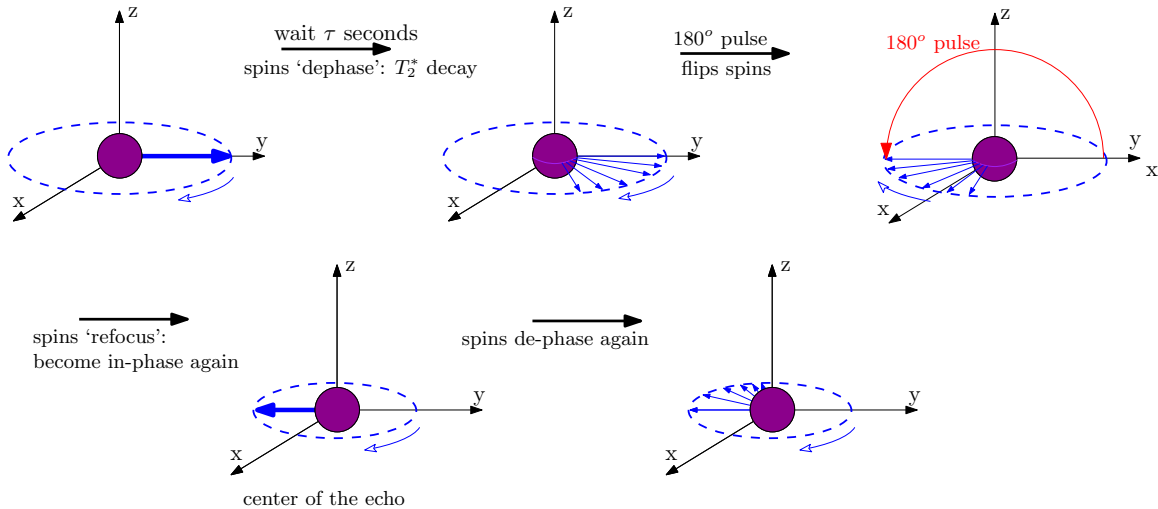


Figure 1-10: Spin-echo diagram.

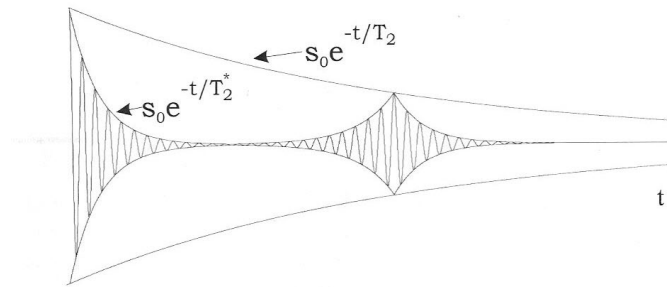


Figure 1-11: Spin-echo signal [8].

1.2.3 Imaging

The fundamental concept that allows us to form images is the fact that the frequency of precession is linearly dependent on field strength. Therefore if we vary the field strength of \vec{B}_0 spatially, we can differentiate signals that corresponds to different points in the sample.

To produce a 2D image of a slice, it is necessary to implement three gradient magnetic coils, which produce magnetic fields that vary linearly in the 3 dimensions.

K-space is a 2D spatial frequency domain that is used in MRI for acquiring data. Sequences involving RF pulses and the gradient fields must be created to transverse and fill k-space. Incredibly, the acquired signal turns out to be the 2D fourier transform of the image! This image corresponds to the signal strength, or proton density

spatially. However, different imaging contrasts can use. For example, images can be formed based on the T_1 or T_2 time constants of the object.

Table 1.1: Relaxation Time Constants Summary

	Longitudinal decay constant: T_1	Transverse decay constant: T_2	FID decay constant: T_2^*
Time constant	Time constant of the exponential rise of M_z to equilibrium.	Time constant of the exponential decay of M_{xy} .	Time constant of the exponential decay of the observed FID.
Physical Reason	M_z exponentially rises as energy is transferred to the lattice, in order for the magnetic moment to re-orient to the lowest potential energy position.	M_{xy} decays as energy is transferred to the lattice, but it can decay faster than M_z rises because of the local magnetic interaction of the spins.	The observed M_{xy} signal (the FID curve) decays faster than the transverse component of individual spins because of B_0 inhomogeneity. The spins dephase because of varying precession speed, and the vector sum of the magnetic moments quickly decays.
Curve	$M_z = M_z(0)e^{-t/T_1} - M_{eq}(1 - e^{-t/T_1})$	$M_{xy}(t) = M_{xy}(0)e^{-t/T_2}$	$M_{FID}(t) = M_{FID}(0)e^{-t/T_2^*}$
How to measure	180-90 or 90-90 sequences can be used. Since only M_{xy} can be measured, M_z is rotated onto the x-y plane. The FID amplitude after the 90° pulse corresponds to the magnitude of M_z at the time of the pulse.	Spin-echo sequences are used to reverse the effects of field inhomogeneity dephasing. The echo amplitude represents the in phase vector sum of the transverse components of the magnetic moments.	An FID curve can simply be observed after a pulse.

1.3 Past Work

Based on the scientific importance of NMR, it is no surprise that there are many sources of past relevant work. Nuclear Magnetic Resonance Imaging is one of the most active areas of research. There are examples of past work that are more relevant to this project because of the use of a low magnetic field or small size.

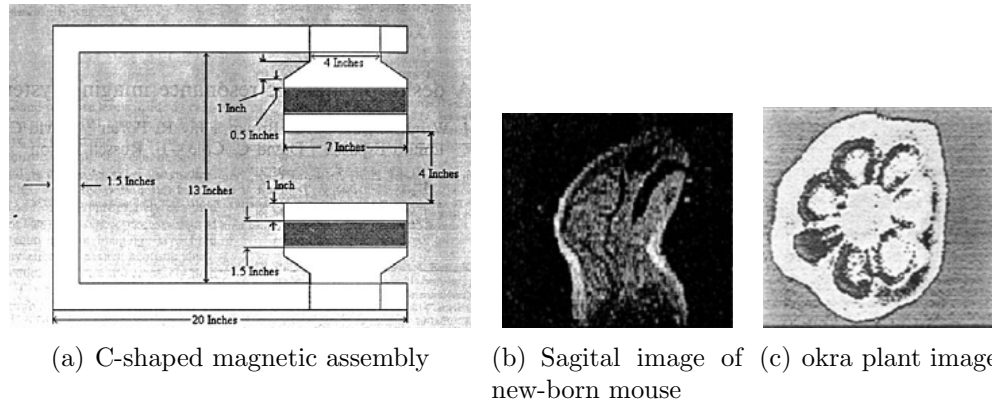


Figure 1-12: Figure of past work in [10]

For example, ‘A Desktop Magnetic Resonance Imaging System’ describes a small desktop MR system developed using permanent magnets and inexpensive RF integrated circuits, at the Magnetic Resonance Systems Lab at Texas A&M [10]. The magnetic setup had a static field of 0.21T and had an imaging region of 2cm. A C-shaped setup was used (as seen in fig. 1-12(a)). In fig. 1-12(b) and 1-12(c) are remarkable images that were formed using the system. This project was done in conjunction with the work described in ‘A Low Cost MRI Permanent Magnet Prototype’ [2]. In [2], the design and construction of a MRI prototype magnet for the C-shape assembly was described. They used several small Neodymium Iron Boron (NdFeB) magnet pieces, and intricately designed pole pieces to form the magnetic circuit. The paper claims that their reason for using several small magnets instead of one large magnet was, “because they are easy to handle, but more importantly because with many pieces we can sort them such that their final stacking contributes most effectively to the field homogeneity”. They used 330 magnet pieces, and characterized them to find the most effective way to stack them.

Some motivating research for this thesis was done in Scotland by JMS Hutchinson in 1980, a developmental time for MRI [4]. In the paper, ‘A Whole Body NMR Imaging Machine’, an early MRI system is described. The remarkable thing about this system is the small static field strength, $\vec{B}_0 = 0.04$ T. Figure 1-13, shows the system and images obtained by the system. The images are low-resolution but would be very instructive to students using the system. The work in [2] served as inspiration for this thesis, as it proved that rough imaging can be done with field strengths that are feasible for classroom use.

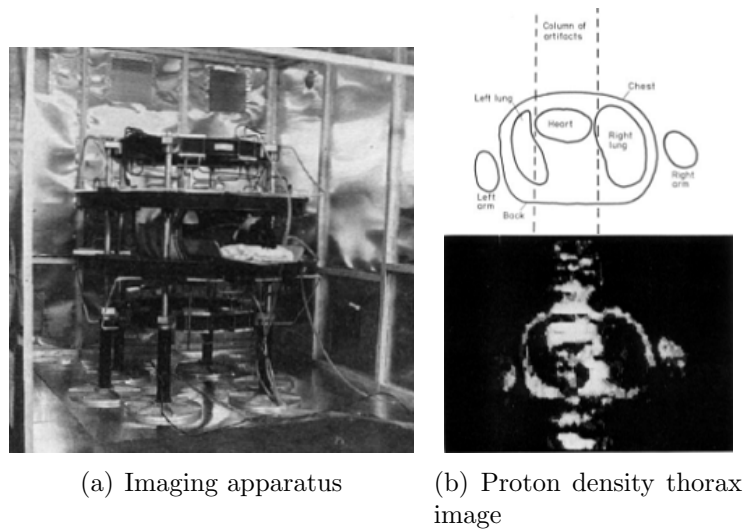


Figure 1-13: Figure of past work in [4]

The most relevant past work for this project was a NMR system developed by J Kirsch at MIT for an undergraduate physics lab [7]. This NMR system, allows students to do pulsed NMR experiments currently at MIT. This system is shown in Figure 1-14. We had access to this system, and it was very helpful in the development of this project.

A laboratory module similar to the system at the MIT undergraduate physics lab was developed at Northwestern University by A Sahakian [1]. The system described in [1] was inspired by the Kirsch’s initial system design at MIT, however, the system in [1] incorporates gradient coils to allow for spatial encoding demonstration. This research motivated some of the permanent magnetic circuit development in our project.

In this thesis, two system designs are described. One uses analog components

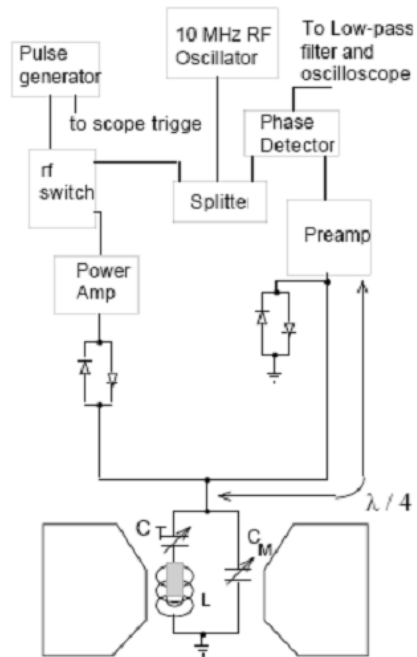


Figure 1-14: Block diagram of the 'Junior Lab' pulsed NMR system at MIT

and a LabVIEW program to generate pulses and process the received signal, this system was mostly for developmental purposes. The second system uses a Field Programmable Gate Array (FPGA) to generate pulses and process the NMR signal.

Two permanent magnetic circuit designs were developed. The first design is similar to the magnetic circuit developed by Sahakian [1], but the second improved design produces a larger and more homogenous field of .133T. The unique probe circuit and adjustable probe holder are also described.

Chapter 2

Pulse Generation and Signal Conditioning Design

There are two overall system designs, one including an FPGA and one including a LabVIEW program. These block diagrams are shown in figures 2-1(a) and 2-1(b).

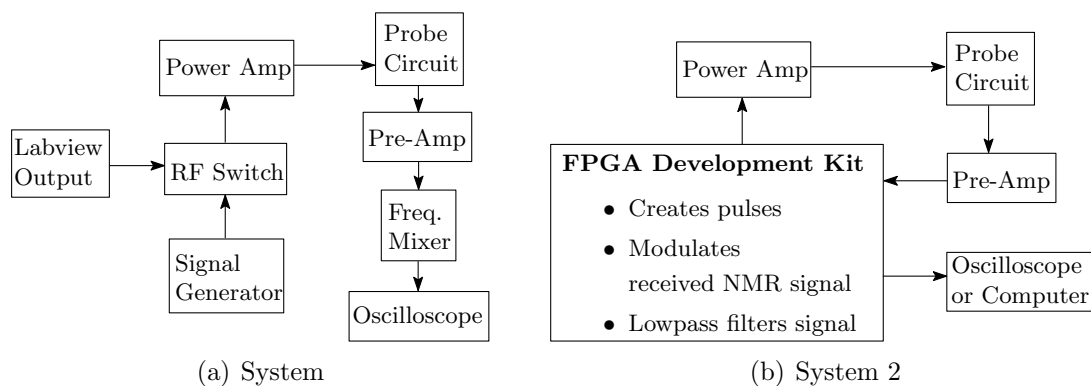


Figure 2-1: Block diagram of the two system designs (without and with the FPGA)

2.1 Design 1

2.1.1 Transmit Chain

In this developmental design, a LabVIEW program is used with a RF switch (Mini-circuits : ZYSW-2-50DR) and a signal generator (Gw Insek SFG-2120) to produce

the pulses. The overall pulse generation process is shown in figure 2-2.

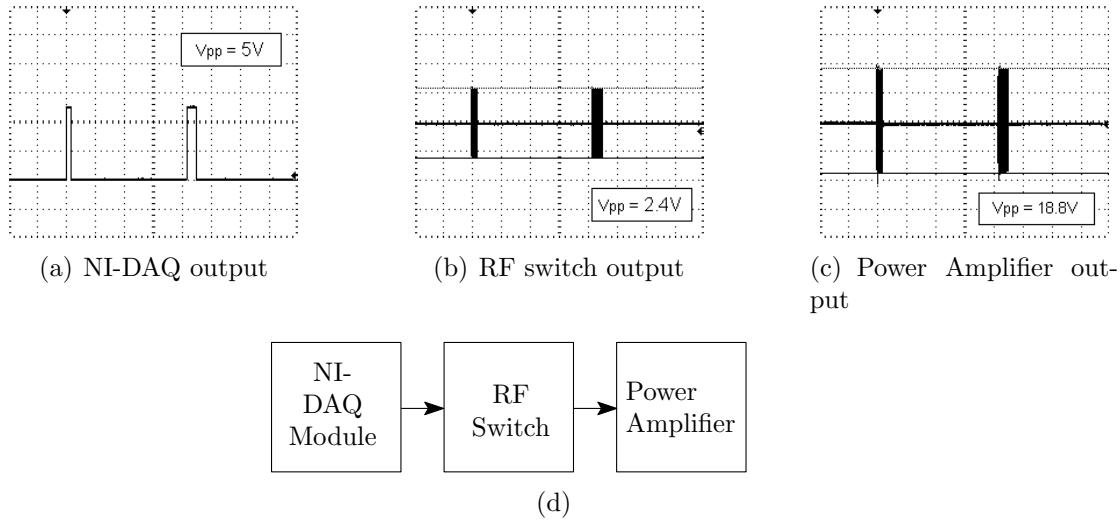


Figure 2-2: Transmit chain in system 1 (no FPGA).

The ‘front-panel’ of the LabVIEW program is shown in figure 2-3, and the LabVIEW ‘block-digram’ is shown in fig. A-1. This program, along with a National Instruments data acquisition module (NI-USB 6212), was used to produce a control voltage that gates the RF switch to make a pulse. The program allows the user to specify the length of two pulses, the time between the pulses (τ), and the repeat time (RT). With the two pulses, the basic relaxation measurement pulse sequences can be created, e.g. spin echo, inversion recovery, and 90-90 sequences.

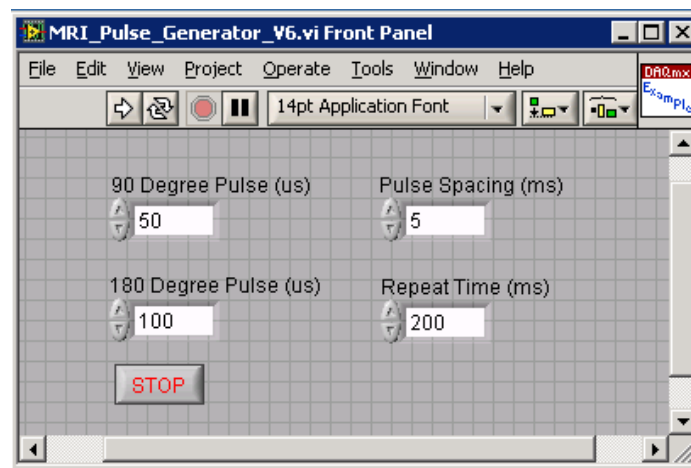


Figure 2-3: LabVIEW front panel of the Pulse Generator program .

An analog output of the DAQ module is used as the control voltage for the RF

switch. This is a single-pole-double-throw absorptive switch with a switching time of 20ns. The switch has four ports: RFin, control, RF1, and RF2. Connected to the RFin port is the signal generator, which produces a sinusoid at the desired frequency and amplitude for the generating the excitation field, \vec{B}_1 . The switch connects the RFin and RF2 ports when the control voltage signal is high. Therefore, the RF2 port produces RF pulses with the frequency and amplitude set by the signal generator and the pulse widths and spacing set by the control voltage (LabVIEW program).

Finally, the pulses are passed through a power amplifier (Minicircuits : ZHL-3A). The power amplifier has a gain of 25dB and has a maximum output of 33dBm. The output of the power amplifier is connected to the probe circuit, where these pulses generate \vec{B}_1 , the RF excitation field.

2.1.2 Receive Chain

NMR signals are generally difficult to observe. This difficulty is due to one of the fundamental issues in NMR: trying to observe a tiny signal in the presence of a relatively large signal (the RF pulse). The RF pulse may be 10^5 to 10^6 times larger than the NMR signal. In order to keep the signal-to-noise-ratio as large as possible, shielding is critical. It is important that all components in the receive chain are shielded and to avoid long leads. In the experimental setup, the longest lead used was the coaxial cable connecting the probe circuit to the amplifier, and it is roughly 1 foot long.

The general receiver design consists of an amplifier, a frequency mixer (which can remove the RF carrier), and a low-pass filter. This design is similar to a superheterodyne receiver. It involves the specific reception and amplification of a narrow band of frequencies, then shifting the frequencies so that they are easier to filter [3]. The receive chain is illustrated in figure 5-6(b).

Figure 2-4(a) shows the initial receive chain signal, which contains the large transmitted RF pulses. Figure 2-4(b) shows the signal after passing through a pair of shunt crossed-diodes which are described in section 2.1.3. At this point the received NMR

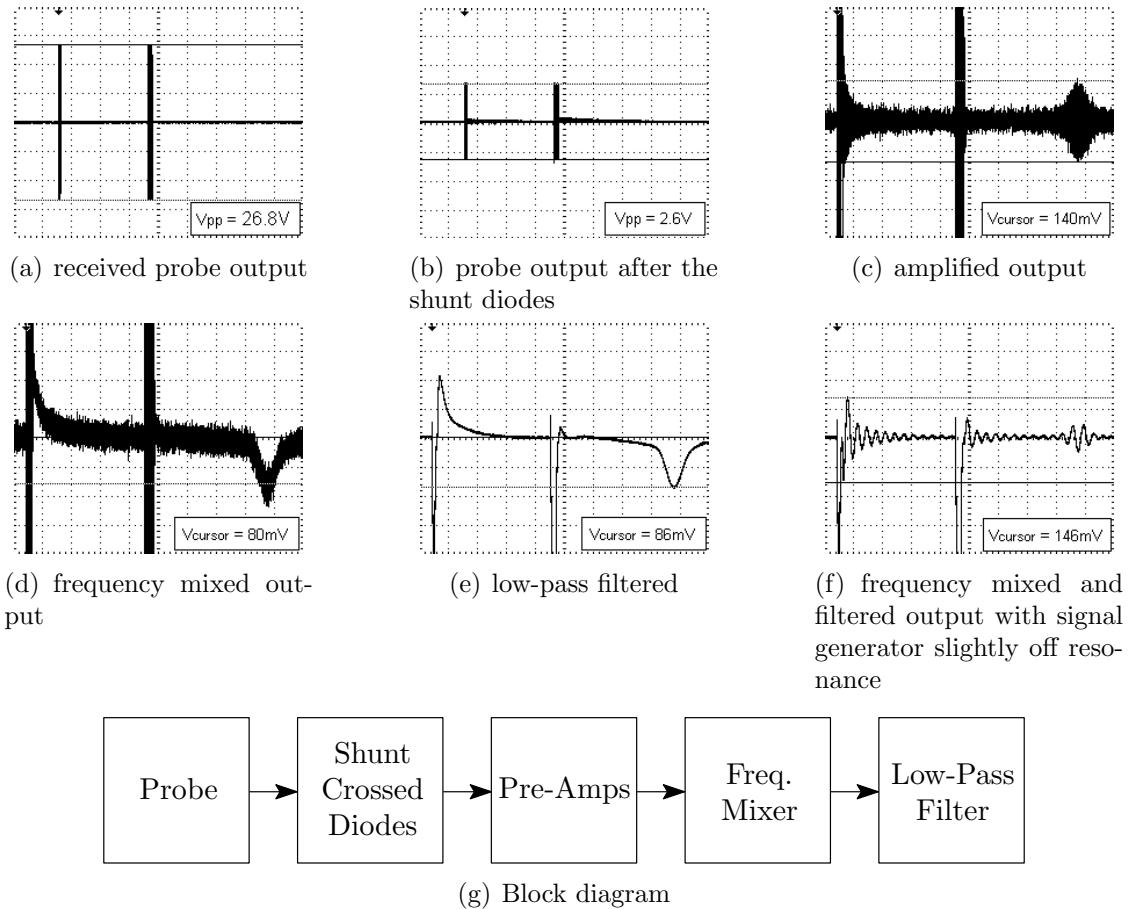


Figure 2-4: Receive chain in system 1 (no FPGA).

signal is amplified to produce the signal in figure 2-4(c)¹. Two cascaded amplifiers were used (Minicircuits ZFL-500LN), which are sensitive ‘pre-amps’ that have a gain of 28 dB and a low noise figure, 2.9 dB.

After amplification we down-modulate the signal using using a frequency mixer (Minicircuits: ZRPD-1), the down-modulated signal is shown in figure 2-4(d). The signal in figure 2-4(d) can be recognized as the envelope of the signal in figure 2-4(c) with some high frequency residue left after mixing. While the NMR signal is in the MHz range, mixing allows us to shift the frequency down and eases low-pass filtering of the signal.

¹These scope-shots were taken using the 2nd version of the magnetic circuit which creates a higher SNR than the 1st version. Because of this we can already see the spin-echo sequence envelope at this point (this is was not possible with the 1st magnetic circuit version). This is described in chapter 3.

In this design (as well as in [7]), the signal generator that was used to produce the pulse is also used to down modulate the received signal. There are two basic options for the signal generator frequency.

1. The frequency may be set to exactly the Larmor frequency of the system. This results in the baseband envelope of the NMR signal. This is shown in figure 2-4(e) (after low-pass filtering).
2. The frequency may be set to be slightly off resonance. This is possible because we can still observe an NMR signal when the pulse frequency is slightly different from the Larmor frequency.² This produces a signal that appears slightly more intuitive because it exhibits oscillation and is not rectified (compare fig. 2-4(e) and 2-4(f)). For example, if the exact frequency of precession is 2.245 MHz, we can set the signal generator to 2.25 MHz to produce a clear NMR signal. The output signal from the frequency mixer will be at 5 KHz (the difference between the frequency of the NMR precessional frequency and the signal generator).

At the relatively low-frequency of the down-modulated signal, it is straightforward to filter the high frequency residue with a simple passive low-pass filter. The filter used here is shown in figure 2-5. It is a simple RC filter with cutoff frequency $f_c = 15.9$ KHz. This filter is contained in a shielded aluminum enclosure (Pomona 2391). After filtering, the NMR signal can now cleanly be viewed on an oscilloscope as shown in figures 2-4(e) and 2-4(f).

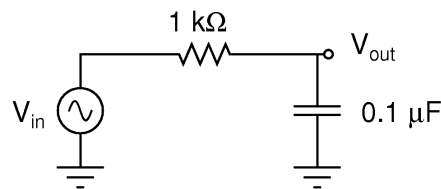


Figure 2-5: Simple passive low-pass filter used to filter high frequency residue from the modulated NMR signal.

²Alternatively, two signal generators could be used. One to produce \vec{B}_1 exactly at the Larmor frequency, and one to mix down the received NMR signal

2.1.3 Isolation

The resonant probe circuit that is shown in the figure 2-1 block diagrams serves two purposes. It transduces the power amplifier signal into the excitation field, \vec{B}_1 , in the sample. It also transduces the NMR field (created by the precessing magnetic moments) into the received electrical signal. Because the coil and probe circuit are used for both the transmit and the receive signal chains, the system must be designed carefully so that the two signal chains are adequately isolated. If the two chains were not isolated the transmitted pulses would damage the sensitive pre-amplifiers which have a low maximum input voltage. It is also important to effectively disconnect the probe circuit from power amp output during the NMR signal observation in order reduce noise [3].

The first attempt to solve this issue was with the use of a second RF switch. The idea was to use the same single-pole-double-throw switch that was used for pulse generation (Minicircuits: ZYSW-2-50DR), with RFin connected to the probe circuit, RF1 connected to the receive chain, and RF2 connected to the transmit chain. However, this was unsuccessful because the switch was unable to pass the high power RF pulses. At the time it was not possible to find another switch that could transmit the pulses (due to their power and frequency frequency characteristics).

The second attempt to solve this issue involved the use of crossed diode pairs for isolation. The resulting circuit is shown in figure 2-6. There are two sets of crossed diodes connected to the probe circuit, including a set in series after the power amplifier and a set of shunt diodes before the pre-amps. The idea is that the received NMR signal will be less than 0.5 volts in amplitude (the conducting voltage for these diodes), and the amplitude of the RF pulses is about 10-20 volts. Therefore, when the pulses are being transmitted all of the diodes will be conducting. The result is the following: the series diodes connected to the power amp are conducting, and the shunt diodes are shunting the pre-amp input to ground. Therefore, the large RF pulses can generate the excitation field in the sample, without damaging the pre-amplifiers. The shunt diodes effectively “damp” the input to the pre-amp to a safe voltage range.

When the pulse is off, this is when we want to observe the NMR signal. During this time, none of the diodes are conducting because the NMR signal is too small. Therefore, there is no conducting path to the power amp and the shunt diodes are not affecting anything. This technique was employed in [1] and [7], and described in [3].

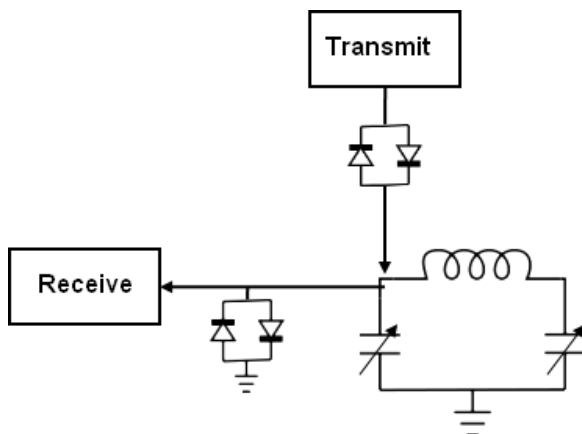


Figure 2-6: The transmit and receive signal chains are isolated with crossed diode pairs.

There are some problems with this isolation design. Specifically, the diodes can distort the signals because they create a dead-zone in the RF pulses (cross-over distortion). The pulses are sinusoidal so there are portions of the signal that are less than 0.5 V where the cross diodes will not conduct. This causes two issues, distortion in the generated excitation field, \vec{B}_1 , and access to the pre-amplifier during those points in the pulses.

To further protect the pre-amplifiers the second RF switch mentioned before can be added. It can be used such that it toggles the connection between the pre-amplifier and the probe circuit (with no connection to the power amplifier output). However, the RF switch slightly attenuates the NMR signal, and the system performs well with only the use of the crossed-diode pairs.

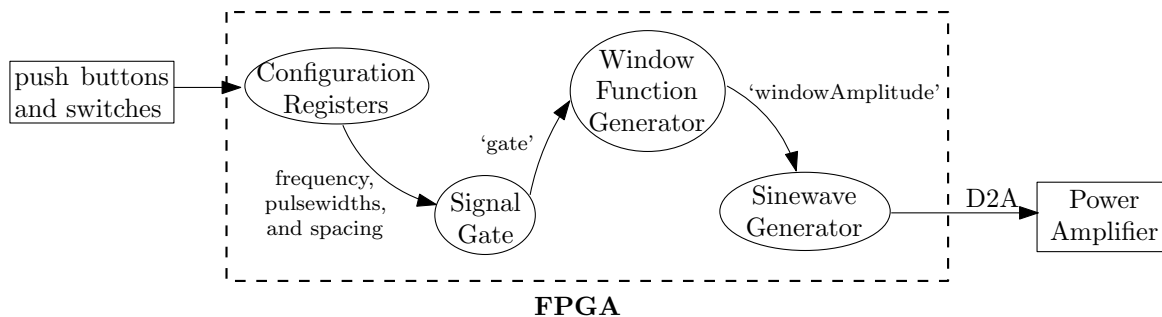
2.2 Design 2

The second system design is similar to the first, except an FPGA (with A/D and D/A converters) replaces some of the components. The product used is the Altera Cyclone III Development Kit (shown in figure 2-7(b)). This includes a variety of LEDs, LCD screens, push buttons, and switches that allows the user to adjust and observe the functionality of the FPGA.

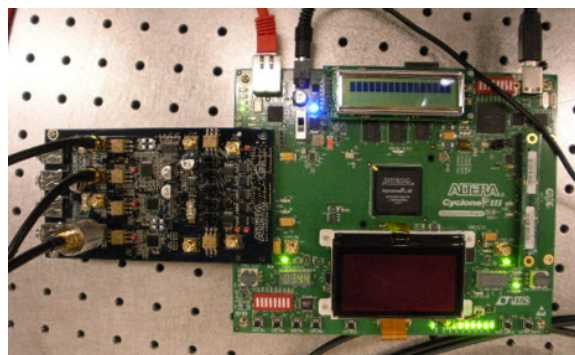
2.2.1 Transmit Chain

The transmit chain is greatly simplified with the use of the FPGA. Verilog code (included in the appendix) was developed to produce the RF pulses. The pulses are output to a D/A converter on a daughter card of the FPGA development kit. While the program is running, the user can use buttons and switches on the development kit to adjust the frequency of the pulses, the pulse widths and the pulse spacing. The output of the D/A converter is again connected to the power amplifier before the probe circuit.

Figure 2-7(a) shows a block diagram of the Verilog modules that are used to produce the pulses. First, the ‘ConfigurationRegisters’ module is used to set the pulse widths, pulse spacing, frequency, and amplitude. Then the ‘SignalGate’ module is used to create square pulses that have the properties that were set in ‘ConfigurationRegisters’. The output of the ‘SignalGate’ module is ‘gate’, which is used as an input to the next module, ‘WindowFunctionGenerator’. This module outputs smoothed pulses (which prevents voltage spiking) and has the output ‘windowAmplitude’. Next, ‘windowAmplitude’ is used as an input to the ‘SinewaveGenerator’ module. The output of this module, ‘signal1’, is a smooth sinusoidal pulse at the desired frequency. ‘signal1’ is passed to a D/A converter then to the power amplifier to produce the RF pulses in this design.



(a) Block diagram of Verilog modules used to produce the pulses



(b) Photo of FPGA Development Kit

Figure 2-7: Transmit chain in system 2 (with FPGA).

2.2.2 Receive Chain

The receive chain of the system is also simplified with the use of the FPGA. After being amplified, the received NMR signal is input to a A/D converter on the development kit. Figure 2-8 shows a block diagram of the Verilog modules used to process the received NMR signal.

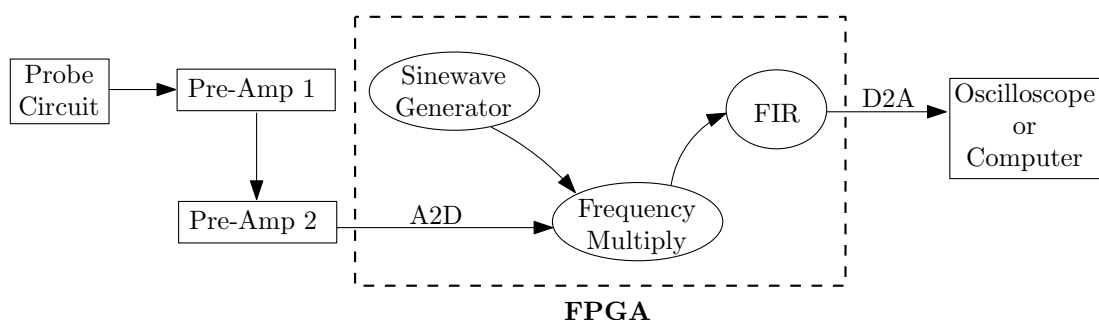


Figure 2-8: Receive chain in System Design 2 (with FPGA).

After being amplified and digitized, the NMR signal, ‘analogsig’, is used as an input to the ‘FrequencyMultiply’ module. Another instance of the ‘SinewaveGener-

ator' module is used to produce the output, 'signal2', this is also used as an input to 'FrequencyMultiply'. The output of 'FrequencyMultiply' is 'demodsinged', which is the result of multiplying the two inputs together. This output is then used as an input to the FIR filter module, 'FIR', which produced the output, 'filteredunsigned'. This filtered output signal is then sent to the D/A converter to be observed with the oscilloscope.

In development is another feature that will allow us to send the filtered output signal to a computer with an Ethernet connection. This function will be highly useful in analyzing signals.

2.2.3 Isolation

The same probe circuit, pre-amplifiers, and power amplifiers are used in this design. Therefore, the transmitter and receiver are isolated in the same way as described for system 1 in section 2.1.3.

Chapter 3

Magnetic Circuit Design and Assembly

The purpose of the magnetic circuit is create \vec{B}_0 , the static magnetic field of the NMR system. It is important that \vec{B}_0 is homogeneous because the frequency of precession is linearly dependant on the field strength.

The original goal for the magnetic circuit design was to obtain a homogeneous magnetic field strength of about 0.1 Tesla within one cubic inch of working volume. Although the idea of using an electromagnet to create \vec{B}_0 was considered, it was decided that use of permanent magnets was a better choice.

The use of electromagnets is simply more difficult because of the need to drive the electromagnet with a large regulated current source. Electromagnets require more utility and power than permanent magnets. Also, depending on the power dissipation in the electromagnet, it might need to be water-cooled. One disadvantage of using permanent magnets versus electromagnets is the impact on system weight. The complete ‘improved magnetic system’, described in section 3.2, weighs about 90lbs. Therefore, the mobility of the system is somewhat limited. Fields created by permanent magnets are also temperature dependent [3]. This means the field can drift over long data acquisitions. Also permanent magnets can only really be used for systems with relatively low field strengths.

Although permanent magnets have some disadvantages, they work well for our

purposes. Temperature drift in the laboratory is not a real issue, and we are interested in having a relatively low field strength. According to [3], permanent magnets are a good choice for fixed field applications where only a moderate field is required, and are much less expensive and easier to maintain than the alternative.

To create a homogeneous field with permanent magnets, it was necessary to create an overall closed magnetic ‘circuit’. The permanent magnets are made of neodymium-iron-boron (NdFeB) and their magnetic field is guided and focused by a ferromagnetic yoke made out of low-carbon steel. SAE 1018 steel was a simple choice because it is lighter than iron, inexpensive, and easily machinable. The use of pole pieces to shape the magnetic field in the gap is necessary to spread the field lines and to obtain a field that is homogeneous in both strength and direction.

Finite-Element modeling software was used to simulate the magnetic circuit designs. Both Comsol¹ and Quickfield² were used. Figure 3-1 shows a variety of magnetic circuit geometries that were simulated using Quickfield. Two versions of the magnetic circuit were built, and will be described.

The assembly of these magnetic circuits is a significant task that should be performed with caution. It is important to carefully plan a procedure for assembly before beginning for two reasons: The first is safety. During assembly, it is not difficult to smash a finger or hand with these small but powerful magnets. During assembly, tough gloves were used as an added precaution. The second reason to plan a procedure is the finality of the assembly. Once the structure is assembled it is difficult to disassemble it.

¹Comsol Multiphysics Modeling and Simulation.

²Quickfield simulation software for electromagnetics, heat transfer and stress analysis

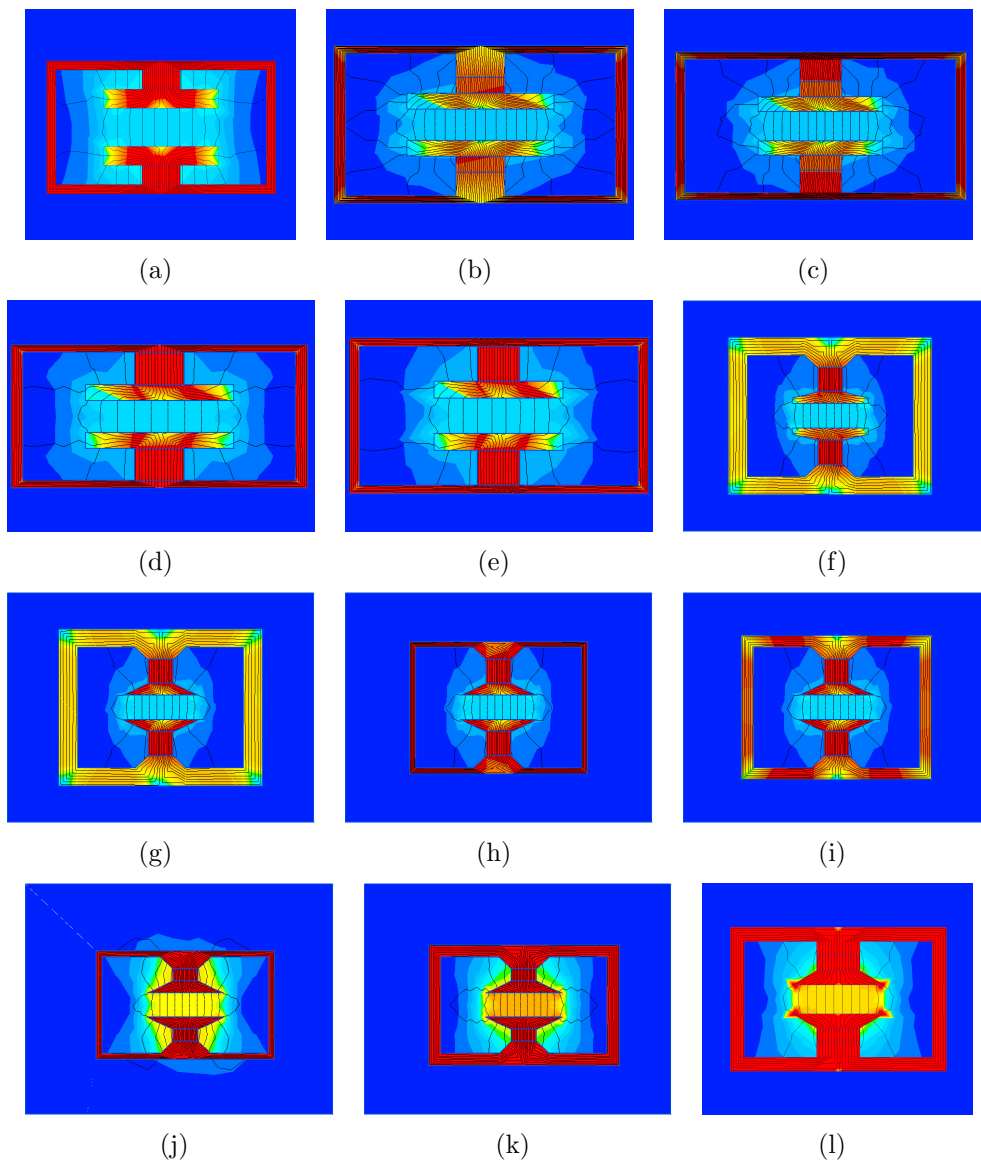
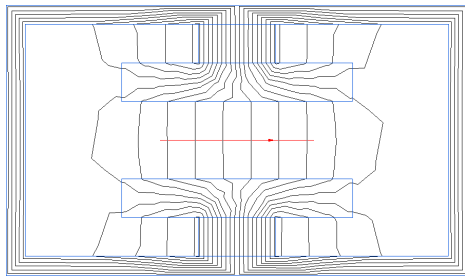


Figure 3-1: Quickfield simulations of a variety of magnetic circuit geometries. The figures show a color map of the flux density and magnetic field lines.

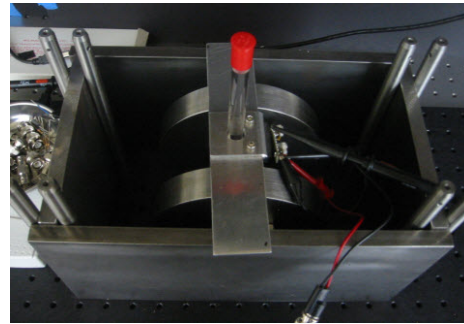
3.1 Preliminary Magnetic System

The first magnetic circuit that was built is in figure 3-1(a). This was built using 2x2x1 rectangular NdFeB magnets. The field was measured using a gaussmeter, and was determined to be 0.0523 T in the center, which corresponds to a Larmor frequency of $f_o = 2.23$ MHz. Figure 3-2 shows a picture of the magnetic setup and a drawing that shows the measured field at various places in the gap. Figure 3-2(a) suggests that this design does use the field most efficiently. After being built, the largest field was measured at the edge of the pole piece, where the field it shunted back to the magnet instead of across the gap.

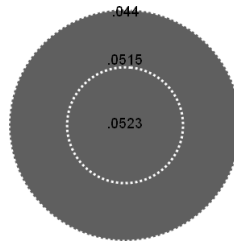
The gaussmeter measurements were slightly inaccurate. When the NMR signal was eventually found with this magnetic design, it was discovered that actual resonant frequency was $f_o = 2.2495$ MHz. According to equation (1.2) this corresponds to a main magnetic field of $\vec{B}_0 = .0528$ T.



(a) Quickfield simulation of design 1 showing field lines



(b) Photo of the preliminary magnetic assembly with probe holder and NMR sample.



(c) Measured field in the center of the gap (the circle represents the pole piece).

Figure 3-2: Preliminary Magnetic System Design

3.1.1 Preliminary Magnetic Design Assembly

The two versions of the magnetic circuit were assembled in different ways. The first way was slightly easier but less permanent and stable.

This magnetic circuit was assembled with the use of some Thorlabs components that were available in the lab. An aluminum optical breadboard was used (Thorlabs: MB1224) and 8 stainless steel post (Thorlabs: TR8). A long scrap magnetic steel piece was also used to assist in the assembly.

Components:

1. 2 rectangular 2x2x1 NdFeB magnets
2. 2 pole pieces: Low-Carbon Steel Rod 6" Diameter, 1" Length (McMaster: 7786T74)
3. 2 Low-Carbon Steel Sheet 1/2" Thick, 6" X 6" (McMaster: 1388K311)
4. 2 Low-Carbon Steel Rectangular Bar 1/2" Thick, 6" Width, 1' Length (McMaster: 8910K714)

Assembly:

1. Separate the magnets: The magnets are packaged separated by plastic rings. Use the edge of a counter-top to push one magnet down to separate them.
2. Mark magnet poles: Each magnet should be marked with an 'A' on side and a 'B' on the other side. (The two 'A' sides should repel each other)
3. Attach the magnets to the pole pieces: This can be done using the scrap steel piece. The pole piece is placed on a large cleared area of the ground. The scrap steel is used to pick up the magnet, and attach it to the pole piece. The magnet and pole piece will slam together, but although the magnet is not exactly in the middle of the pole piece this can be fixed. One pole piece should be attached to the 'A' side of one magnet, and the other pole piece should be attached to the 'B' side of the other magnet. Keep the two attached magnet and pole pieces far

apart from each other. It is not too difficult to slide the magnet to the center of the pole piece once it is attached. However the magnet will move again during the assembly process so this adjustment may be rough for now.

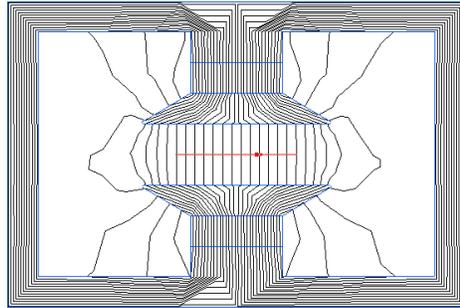
4. Attach magnets to the long rectangular sheets: This may be done by hand (with gloves of course). The steel sheet should be placed on the floor. The assembler can stand on the steel sheet to hold it down while lowering the magnet and pole piece onto it.
5. Adjust the alignment: It is a good idea to adjust the alignment of the magnet and pole piece at this point. The magnet should be exactly in the middle of both the pole piece and the rectangular sheet. Slight offsets can greatly affect the homogeneity of the magnetic field.
6. Assemble the box: The stainless steel posts are attached to the breadboard, as shown in the photo (fig. 3-2(b)), to hold the steel sheets during the assembly. At this point there are two assemblies (poles piece, magnet, and steel sheet). One of these assemblies should first be placed on the bread board as shown in the photo. Then, the posts and side pieces of the box should be carefully attached. Finally the second assembly should be carefully attached, completing the box.

3.2 Improved Magnetic System

This second magnetic system was designed and constructed after the preliminary magnetic system was built and functioning as an NMR system. The problems with the preliminary magnetic system were taken into account in this second system.

The second magnetic system is shown in figure 3-1(l). This improved magnetic circuit design was built using 3" diameter cylindrical NdFeB magnets. The rectangular low-carbon steel box was welded together. Cylindrical spacers and slanted pole pieces were used. Figure 3-3 shows a photograph of this magnetic design and the measured field. The measured field in the middle of the gap was $B_0 = 0.131$ T, which

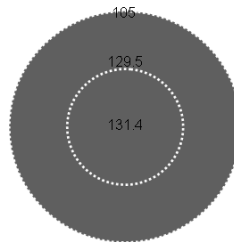
corresponds to a Larmor frequency of $f_o = 5.58$ MHz. However, the measured field from the gaussmeter was again lower than the actual field. When the NMR signal was found it was discovered that the Larmor frequency is actually $f_o = 5.668$ MHz, which corresponds to a static field strength of $\vec{B}_0 = 0.133$ T.



(a) Quickfield simulation of design 2 showing field lines, and the cross section line that corresponds to figure.



(b) Photo of the design 2 magnetic assembly with probe holder and NMR sample.



(c) Measured field in the center of the gap (the circle represents the pole piece).

Figure 3-3: Improved Magnetic System Design

3.2.1 Improved Magnetic Design Assembly

This assembly was made more permanent and solid than in the preliminary design. The low-carbon steel used for the rectangular box is thicker, 1" pieces are used instead of 0.5" pieces, and these pieces are welded together. A machine shop was hired to weld and machine the pieces necessary for this design³. SolidWorks drawings in figure B-1 and B-2, show the received pieces. The assembly description here is less detailed than that for the preliminary magnet to avoid redundancy.

³Eastern Tool Corporation, Medford, MA

Components:

1. Low-carbon steel box. 15"x10"x6" 1" thick steel pieces (fig. B-1)
2. 2 Spacers: 3" diameter 1" thick low carbon steel disks
3. 2 Magnets: 3" diameter 1" thick NdFeB magnets
4. 2 slanted pole pieces (fig. B-2)

Assembly:

1. Separate the magnets.
2. Label the poles of the magnet.
3. Attach pole pieces: This was done more carefully than for the first assembly. Two 2x4 pieces of wood were used to hold down the pole piece to the floor while the magnet was attached. Two people stood on the pieces of wood to hold down the pole piece. A third person used the scrap piece of steel to attach the magnet to the pole piece. Again, one pole piece was attached to the 'A' side of one magnet, and the other pole piece was attached to the 'B' side of the other magnet.
4. Attach the spacer pieces: This was done very cautiously, while the pole pieces and magnets were held down on the floor as described above. It was not possible to use the steel scrap piece for this part. The third person carefully held the top of the spacer while lowering it to the magnet. Again, the components were carefully aligned later.
5. Attach the pieces to the steel box: The first assembled piece was lowered into the box fairly easily. This is because there was plenty of room in the box. The second piece was a little trickier. This was done by putting a piece of wood between the two pole pieces and sliding the second pieces into the box.

3.3 Magnetic Design Comparison

The improved magnetic design performs better than the preliminary design because the field strength is more than twice as large and is more uniform. Having a stronger static field, \vec{B}_0 , increases the signal strength for two reasons:

1. The increased field causes a greater majority of magnetic moments to align with the field, which increases the magnitude of the net magnetization vector, \vec{M} .
2. The generated emf in the receive coil is proportional to the time-derivate of the magnetic flux. Therefore, faster precession, which results from a higher field, increases the received signal strength.

In figure 3-2(a) and 3-3(a), there are red lines across the middle of the gaps. The simulated fields are plotted for these cross-sections in figure 3-4. Figure 3-4 compares the two simulated field strengths and uniformity.

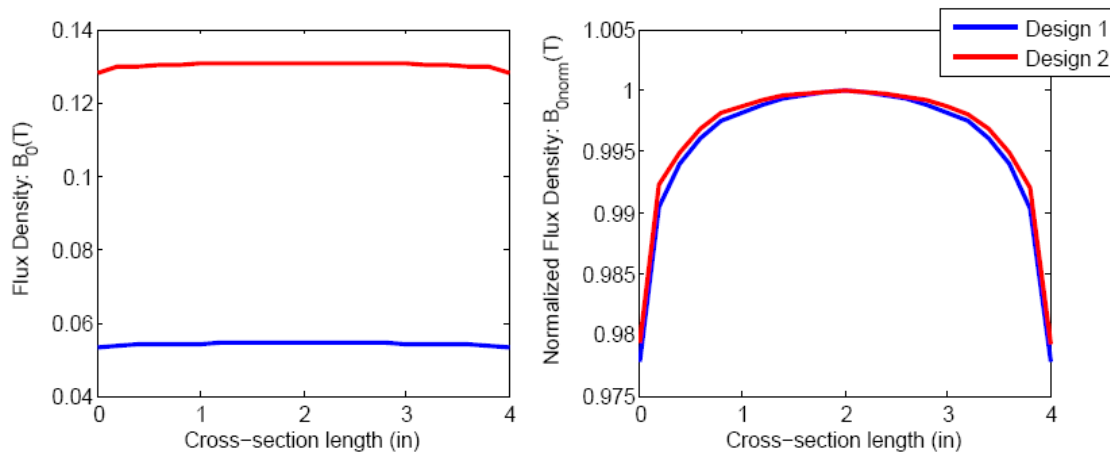


Figure 3-4: Comparison of simulated field in the preliminary magnet and improved magnet designs.

The superiority of the second magnetic design, was clear from the measured signal strength. Using system design 1 (no-fpga), an FID amplitude of about 15mV was obtained from the preliminary magnetic design, while an FID amplitude of about 120mV was obtained from the improved magnetic design.

Chapter 4

Probe Design

The developed NMR systems use a single solenoid as both a transmitter and receiver. The coil is used to create \vec{B}_1 , the excitation magnetic field, and also to detect the NMR signal.

4.1 Transmit/Receive Coil Background

The coil is used to create \vec{B}_1 by driving it with an RF current, as is explained by Ampere's law. The integral form of Ampere's Law is

$$\oint_C \vec{B} \cdot d\vec{s} = \mu_0 \iint_A \vec{J} \cdot d\vec{a}, \quad (4.1)$$

where \vec{B} is the induced field and J is current density. Figure 4-1 illustrates the generation of the excitation field in a solenoid. In Figure 4-1 a cross section of a solenoid is shown, where the circles represent the cross-section of wires. The circles with dots represent current out of the page, and the circles with x's represent current into the page. The solenoid has N turns, and the length of the solenoid is ℓ . The generated magnetic field is \vec{B} . The direction of the field follows the right-hand rule.

The left side of equation (4.1) represents the integral of the magnetic flux density along a contour (e.g. C_1 or C_2 in figure 4-1). The right side of (4.1) represents the total current through the contour. Let us first consider contour C_1 , which encircles

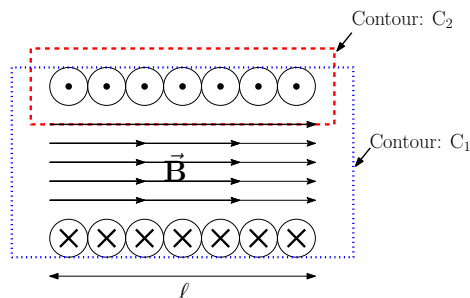


Figure 4-1: Demonstration of Ampere's Law in a solenoid.

the current into the page and out of the page. The net current encircled by C_1 is zero. Therefore, according to ampere's law the contour integral of \vec{B} should also be zero. We can assume for now, then, that the flux density outside the coil is zero ($B_{out}^{\vec{}} = 0$) which is consistent with (4.1). The second contour, C_2 only encircles the current out of the page, and therefore has a net current of

$$\int \int_A \vec{J} \cdot d\vec{a} = Ni(t). \quad (4.2)$$

The left side of (4.1) is a dot product of the field and the contour. This is only non-zero when \vec{B} is parallel with the $d\vec{s}$. With the assumption that $B_{out}^{\vec{}} = 0$, the left side of (4.1) is only non-zero inside the solenoid and simplifies to

$$\oint_C \vec{B} \cdot d\vec{s} = B\ell. \quad (4.3)$$

Therefore, the \vec{B} created by the coil is

$$B = \frac{N\mu_0 i(t)}{\ell} \text{ A/m}. \quad (4.4)$$

The coil is also used as an antenna to detect the NMR signal. As it is explained in section 1.2, the magnetic moments in the sample precess about the \hat{z} axis, and when the magnetization is perturbed from equilibrium, a transverse magnetization component exists. This means that the magnetic flux of the large number of small magnetic moments is rotating about the \hat{z} axis. According to Faraday's Law, when a magnetic flux is swept through a coil, an emf is generated. On a much larger scale

this is the same way electrical generators work. Thus the precessing spins induce a voltage across the probe coil that can be measured.

The integral form of Faraday's Law is

$$\oint \vec{E} \cdot d\vec{l} = -\frac{d\Phi_B}{dt}, \text{ where} \quad (4.5)$$

$$\Phi_B = \int \int_A \vec{B} \cdot d\vec{a}. \quad (4.6)$$

\vec{E} is the electric field, \vec{B} is the magnetic field, and Φ_B is the magnetic flux. For the simple case of a single turn loop of wire these concepts are illustrated in figure 4-2. In fig. 4-2, the dashed line is the contour to which the equations apply and the small circles represent the magnetic field lines out of the page.

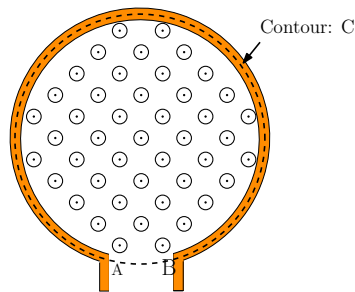


Figure 4-2: Demonstration of Faraday's law in a loop of wire.

Since the electric field in a perfect conductor is zero, the left side integral in (4.5) represents the integral of the electric field from point A to B in figure 4-2. This is equal to the voltage or emf across the coil,

$$emf = \int \vec{E} \cdot d\vec{l}. \quad (4.7)$$

The right side of (4.5) represents the time derivative of the integral of the magnetic flux density through the surface of the contour. Therefore, the emf generated around the wire loop is equal to the negative time derivative of the magnetic flux through the loop,

$$emf = \frac{-d\Phi_B}{dt}. \quad (4.8)$$

In the case of a solenoid, a coil of wire with several loops, the generated voltage is higher. This is because the total voltage across the solenoid is equal to the sum of the emfs generated around each loop of wire. Therefore, if the solenoid has N turns, the voltage across the solenoid is

$$emf = N \frac{-d\Phi_B}{dt}. \quad (4.9)$$

The field produced by the transverse component of the precessing spins can be represented as:¹

$$\vec{B}(t) = -B \sin(\omega t) \hat{x} + B \cos(\omega t) \hat{y} \quad (4.10)$$

By substituting this into equation 4.5 we get:

$$emf = NAB\omega \cos(\omega t) \quad (4.11)$$

This is the induced emf across the solenoid, where A is the the cross sectional area of the solenoid [8]. Note that there is a factor ω in (4.11) which indicates that the induced emf is proportional to the precessional frequency and thus \vec{B}_0 .

A resonant circuit is generally used to detect the NMR signal because a resonant circuit only allows the detection of a narrow frequency band, which can be tuned to the Larmor frequency of the system. This results in a high degree of frequency specificity. The resonant circuit design is an LC tank circuit, in which the transmit/receive coil serve as the inductor. The circuit should be designed for optimal performance at the Larmor frequency of the system. It should be able to efficiently perturb the spin's magnetization and to also detect the resulting transverse precession [8].

4.2 Coil Design

The solenoid was designed with physical and electrical constraints in mind. It was designed so that an NMR test tube could fit snugly in the coil, and so that the

¹Note: this equation does not incorporate relaxation

inductance was a reasonable value for the design.

According to [3], there are several factors to consider when designing the probe and probe holder. For example, the probe enclosure should be rigid to avoid microphonics (mechanical motion that results in a signal by changing the capacitances), and none of the components should be ferromagnetic (including capacitors). Also, it is desirable for the coil to be directly wound around the sample because this results in better signal-to-noise ratio (SNR).

The quality factor (Q) of the coil and the resonant circuit involves a trade off. On one hand, a large Q results in a large signal-to-noise ratio (SNR) because the resonant circuit acts as a bandpass filter. On the other hand, a high Q also means a longer ring-down time (longer system recovery time from the pulses).

$$Q = \frac{2\pi\omega_o L}{R} \quad (4.12)$$

Clearly from equation (4.12), the quality factor is proportional to inductance and inversely proportional to the resistance of the coil. This is a trade-off in itself because a larger inductance is achieved with more turns of the solenoid. However, more turns means more wire and often means smaller wire diameter (if one constrains the length of the coil). Both of these things result in a higher resistance.

The inductance of a solenoid can be derived using Faraday's law and Ampere's law. If we substitute the generated field in equation (4.4) into the equation for magnetic flux (4.6), we get

$$\Phi_B = \int \int_A \vec{B} \cdot d\vec{a} = \frac{NA\mu_o i(t)}{\ell}. \quad (4.13)$$

Now if we substitute expression (4.13) into the expression for induced emf in a solenoid (4.9), we get the voltage-current relationship for an inductor,

$$emf = N \frac{-d\Phi_B}{dt} = \frac{\overbrace{N^2\mu_o A}^L}{\ell} \frac{di(t)}{dt}. \quad (4.14)$$

From this constitutive relationship we can extract the expression for the inductance

of a solenoid [11],

$$L = \frac{N^2 \mu_o A}{\ell}. \quad (4.15)$$

The coil was made using AWG 20 magnet wire wrapped around a test tube, this is shown in figure 4-3. The wire was tightly wound, and then epoxy was used to hold it together.



Figure 4-3: Photo of a coil being made.

Several coils were wound and tested. The one that was finally used for the preliminary design had an inductance of $L = 3.18\mu H$. Table 4.1 describes the coil properties.

Table 4.1: Coil 1 Properties

Radius(r)	.75cm
Length(l)	1.9cm
Turns(N)	20
Wire (AWG)	20
Calculated Inductance	$4\mu H$
Measured Inductance at @2.25 MHz	$3.18\mu H$
Resistance at @2.25 MHz	$.4\Omega$

The properties of the coil currently used in the improved magnetic system are shown in table 4.2. This coil has the same number of turns and roughly the same length and cross-sectional area as coil 1. However, this coil has a higher inductance, $L = 3.44\mu H$. This is probably due to the neatness of the coil and the orientation and length of the leads.

Note that the inductance and resistance of the coils were measured at the intended operating frequency. This is especially important for the resistance measurement

Table 4.2: Coil 2 Properties

Radius(r)	.75cm
Length(l)	1.9cm
Turns(N)	20
Wire (AWG)	20
Calculated Inductance	4 μ H
Measured Inductance @5.667 MHz	3.443 μ H
Resistance at @5.667 MHz	2.7 Ω

because at high frequencies skin effect in the wire becomes significant, effectively increasing the resistance.²

4.3 Probe Circuit Design

The design of the probe circuit is a series LC tank circuit, consisting of L (the inductance of the coil) and C_t (the tuning capacitor). At the resonant frequency of the tank circuit it has a low impedance, Z_{in} . The impedance of the inductor and capacitor have opposite signs ($+i\omega L$ and $-i/\omega C$), so at a specific frequency (the resonant frequency) their impedance cancel. Therefore, the impedance at the resonant frequency is equal to the parasitic resistance in the circuit components.

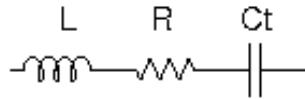


Figure 4-4: A series LC tank circuit, including the intrinsic resistance of the inductor.

It is also necessary to match the impedance of the probe circuit to the other components (e.g. the pre-amplifier and power amplifier) to achieve maximum SNR. For example, the input impedance to the pre-amp is 50 Ω . If the output impedance of the probe circuit is not 50 Ω , the power transfer will be suboptimal. A matching

²skin effect means that the current remains on the surface of the conductor thereby under-utilizing the wire diameter.[6]

capacitor, C_m , is added in parallel so that the total input impedance at the resonant frequency may be 50Ω . In figure 4-5, C_m is the matching capacitor, L is the coil, R is the intrinsic and added resistance, and C_t is the LC tank capacitor which henceforth will be referred to as the tuning capacitor.

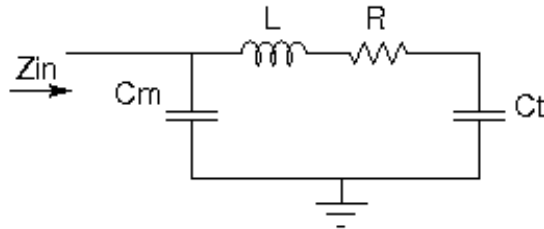


Figure 4-5: Schematic of the resonant circuit with tuning and matching capacitors.

With fixed values of ω and L , the values of C_t and C_m were calculated so that at the resonant frequency, $Z_{in} = 50\Omega$ (the imaginary part of the input impedance must be zero for resonance):

$$C_t = \frac{1}{L\omega^2 - \omega\sqrt{50R - R^2}} \quad (4.16)$$

$$C_m = \frac{L - \frac{1}{C_t\omega^2}}{R^2 + \left(\omega L - \frac{1}{\omega C_t}\right)^2} \quad (4.17)$$

Table 4.3 shows the calculated capacitor values for the two systems.

Table 4.3: Calculated tuning and matching capacitor values.

	Magnet 1	Magnet 2
Larmor Freq. (MHz)	2.25	5.668
Coil Inductance (μH)	3.18	3.443
Coil Resistance (R)	.4	2.7
Tuning Capacitor (pF)	1880	250
Matching Capacitor (pF)	6200	2100

The tuning capacitor, C_t , and matching capacitor, C_m , are both adjustable. Trimmer capacitor were used with a range of 12pF - 120pF (Johanson Manufacturing part: 9328) in addition to larger ceramic capacitors. There are several possible sources of parasitic capacitance in the probe assembly (including the capacitance between the coil windings) that can affect the behavior of the resonant circuit. Their may also be

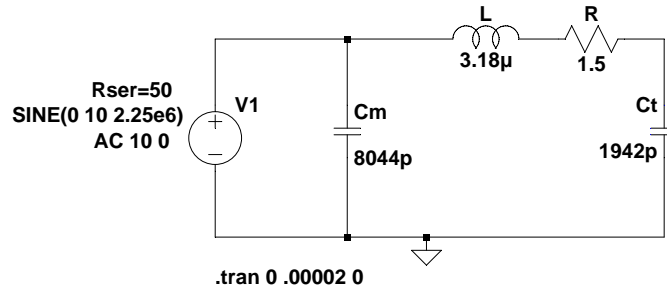
slight variation in the desired resonant frequency due to temperature drift of the magnets or the location of the probe in the magnetic field. Having adjustable capacitors allows us to account for all of these things by allowing a 100pF range of adjustment. When the entire NMR system is implemented, these capacitors can be adjusted until the maximum NMR signal is achieved.

Figures 4-6 and 4-7 show the simulation of the two probe circuits in use. Figures 4-6(a) and 4-7(a) show the schematics of the simulated circuits in LTspice. Figures 4-6(b) and 4-7(b) are the result of an ‘ac analysis’ simulation. The resonant peaks of both circuits are obvious, and are exactly at the desired frequency. Figures 4-6(c) and 4-7(c) are the result of a ‘transient simulation’. The purpose of this simulation is to demonstrate the impedance matching of the circuit. In the circuit schematics, the input voltage source has an amplitude of 10V and a source impedance of 50Ω. If the input impedance of the probe circuit is 50Ω then the voltage across C_m should be half of the source amplitude (like a voltage divider). This is clearly the case in the transient simulations, where the voltage amplitude at the probe circuit input is about 5V.

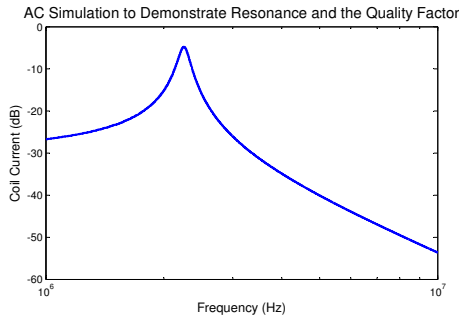
After the the \vec{B}_1 pulse is applied there is always some dead-time before the NMR signal can be observed. This can be due to receiver paralysis (from feed-through of the high voltage RF pulse and the system ring-down. Ring-down occurs after the pulse is off, but energy is still resonating in the circuit. This is problematic because it can easily obscure the small NMR signal. According to [3], “the RF excitation due to the transmitter pulse will take about 20 tank circuit time constants to decay to amplitudes comparable to NMR signals”. Without the addition of additional circuitry³, the solution to this problem is a lower quality factor.

The advantages of a high quality factor are irrelevant if the signal cannot be detected because it is obscured by the ring-down transient. Additionally, a lower Q could allow more flexibility. It could be useful in searching for the resonance of new system because a lower quality factor leads to less frequency selectivity. The quality factor is easily reduced by adding resistance to the resonant circuit, or decreasing the

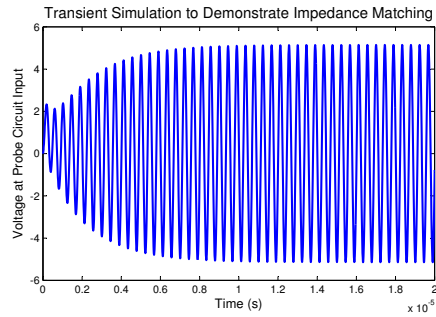
³Another solution is to add a ‘Q-spoiler’, which adds damping to the circuit after the pulse



(a)



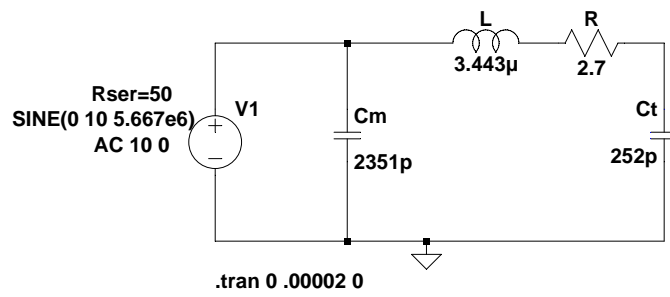
(b)



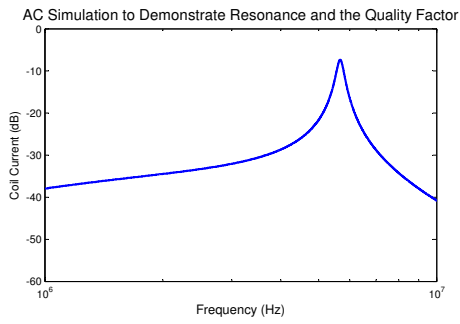
(c)

Figure 4-6: Preliminary magnetic system probe circuit simulation

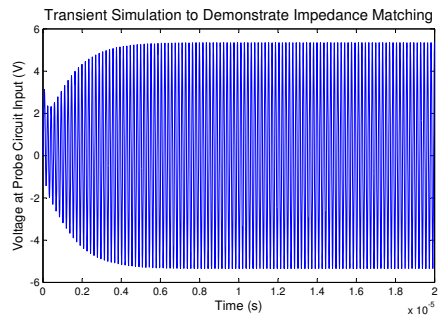
inductance. For these reasons, a 1Ω resistor was added to the first probe circuit. The probe circuit for the preliminary magnet design has a quality factor of $Q = 15$. The probe circuit for the improved magnet design has a quality factor of $Q = 23.1$. These quality factors are relatively low, but lead to sufficient signal detection. These values seem to be a good compromise between signal strength and ring-down time.



(a)



(b)



(c)

Figure 4-7: Improved magnetic system probe circuit simulation

Chapter 5

Results

5.1 Experimental Implementation

5.1.1 System assembly

The mechanical assembly of the magnetic circuit is described in chapter 3. The rest of the system assembly will now be described.

Probe Circuit and Probe Holder

The probe circuit was laid out in PCB Artist and is shown in figure 5-1. Although the power amplifier is separated from the probe circuit with external series crossed diodes, a pair of crossed diodes is also added to the printed circuit board (PCB) to separate the transmit and receive lines.

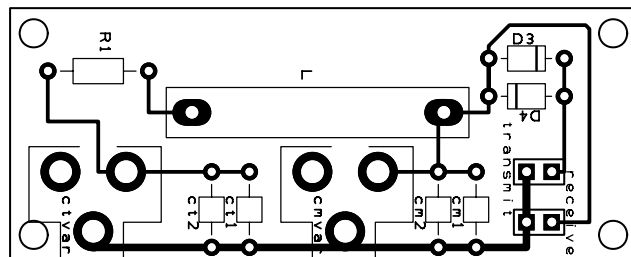


Figure 5-1: PCB layout the probe circuit

The mechanical assembly of the probe holder is shown in figure 5-2. The probe holder consists of the following parts (which are almost all made from aluminum):

1. 2 aluminum project boxes (Bud Industries: CN-5702)
 - (a) one holds the coil with a test tube size hole drilled in top
 - (b) the other holds the probe circuit PCB, and has 2 sma connectors attached to the top (POMONA: 72961)
2. A double dovetail rotating clamp (Thorlabs: XT34RD)
3. A double dovetail clamp (Thorlabs: XT34C2)
4. A raw dovetail extrusion (Thorlabs: XT34RL2)
5. A dual profile dovetail extrusion (Thorlabs: XT34RD)

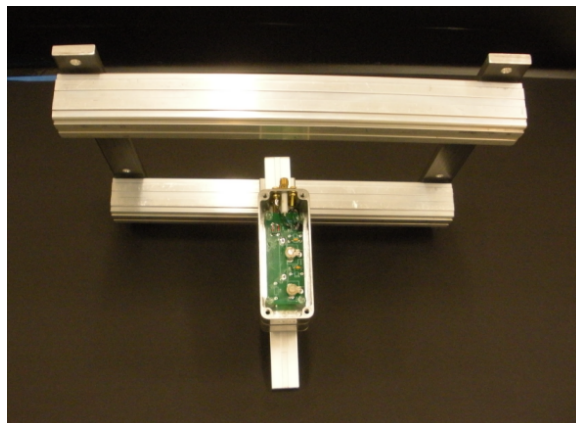
The two small aluminum project boxes hold the PCB and the coil, and are attached together. One of the project boxes has 2 sma connectors attached to the top, which are connected to the transmit and receive lines. The other project box has a test tube size hole drilled in the top that allows the sample to sit in the coil.

These boxes are attached to a vertical dual profile dovetail aluminum extrusion. It is attached with a double dovetail clamp, which allows the box to easily slide up and down the extrusion for adjustability. A square brace was constructed that sits on top of the magnetic assembly with raw pieces of aluminum and square raw dovetailed extrusion. The vertical extrusion is attached to the square brace with a rotating clamp, that allows angular adjustability of the probe.

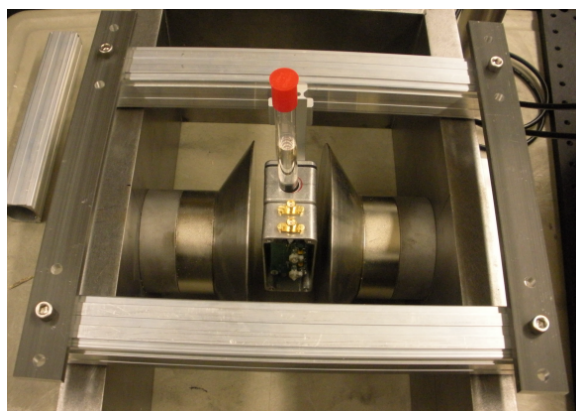
Other Components

The other components for the system were enclosed in an aluminum box, with BNC connectors attached to ensure shielding and stability. This is shown in figure 5-3.

The Minicircuit components used in the NMR system require various supply voltages. The power amplifier requires a 24V supply, the pre-amps require a 15V supply,



(a) Photo of probe holder assembly.



(b) Photo of probe holder assembly in the improved magnetic design (with NMR sample inserted).

Figure 5-2: Photos of probe holder assembly.

and the RF switch requires a $\pm 5V$ supply. To accommodate these components, a single dual-output power supply was used along with linear voltage regulators. The ‘power supply board’ is shown in figure 5-4.

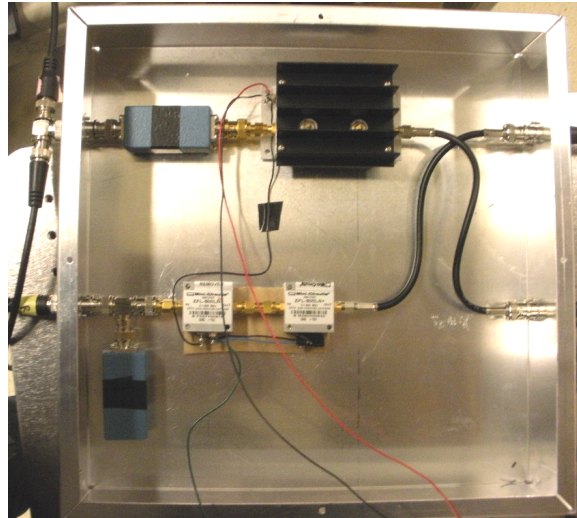


Figure 5-3: Photo of the electronic components box.

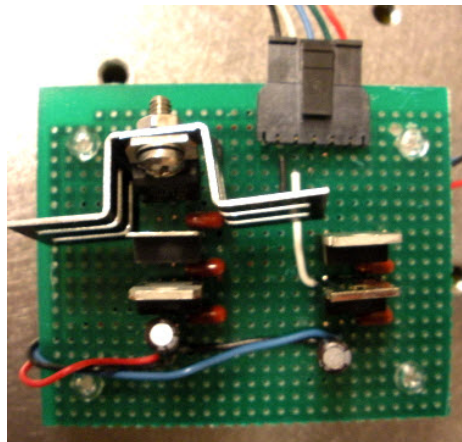


Figure 5-4: Photo of the 'power supply board'.

5.1.2 Implementing Experiment

One of the most challenging steps in building a working NMR system is initially finding the NMR signal. The fundamental difficulty of NMR is being able to detect an extremely small signal after inducing a large signal. In addition to this difficulty, the ability to find a signal is dependent on several independent variables: probe position, frequency, capacitor tuning, and pulse amplitude and duration. Finding the correct combination of the variables is not trivial.

To find a signal, it is necessary to have a good guess of the independent variables to begin with. This guess can be made by measuring the field to estimate the Larmor frequency. Because the signal is likely to be small to begin with, a sample that yields a high SNR should be used. A 100% glycerin sample was used when searching for a signal and for the experiments. Glycerin produces a large NMR signal because it has a high hydrogen content and viscosity. ¹.

In order to find a signal with the preliminary magnetic structure, it was discovered that more amplification, more shielding, and adjustability of the probe holder was needed. These lessons were applied to the improved magnetic structure, and a more repeatable procedure for finding an NMR signal was followed:

- A gaussmeter was used to measure B_0 . The field measurement with the gaussmeter was not accurate enough to find the exact Larmor frequency of the system, but it provided a good starting point of $f_o = 5.58MHz$.
- The inductance and resistance of the coil was measured at the approximated Larmor frequency with an LCR meter.
- The measured inductance, resistance, and estimated f_o were used to calculate the tuning and matching capacitor values (as shown in section 4.3).
- The probe circuit PCB board was populated and the probe holder was assembled.

¹Glycerin has short time constants compared to water because of its viscosity. A short T_1 generally leads to a larger signal [3]

- The experimental setup was connected as shown in the ‘System 1’(no FPGA) configuration (5-5). The ‘System 1’ configuration is easier to use when searching for resonance, because it allows more flexibility and transparency. An oscilloscope was used to monitor the receive chain at 2 stages and the transmitted pulse.
- The signal generator was set so that the output sinusoid was $f = 5.58$ MHz and the transmitted pulse was around 15V amplitude. The LabVIEW pulse generator program was set so that the pulse widths were fairly long, $50 - 100 \mu\text{s}$.
- At this point, shielding with aluminum foil was applied around the probe holder to reduce unwanted pickup at the receiver output. When searching for the initial NMR signal, it is necessary to reduce extraneous signals as much as possible because the signal is likely to be very small at first.
- The frequency of the signal generator was swept very slowly through a 100KHz range around the estimated f_o . The first several times this was done, no signal was visible. One variable at a time was adjusted before sweeping through frequency again. For example, the tuning capacitor was rotated 1/4 of a turn or the probe holder was adjusted to change the sample position in the magnet.
- After several adjustments (and several days) a very small wiggle (about 2mV) was observed at the receiver output at $f = 5.667\text{MHz}$. This pinpointed the exact Larmor frequency and static field strength, $B_0 = .133T$. At this point, it became relatively easy to make adjustments that increased the signal strength. For example, capacitor values were changed, the variable capacitors were adjusted, and the probe position was adjusted. The maximum signal strength achieved was 140mV, which corresponds to about $400\mu\text{V}$ in the probe circuit.

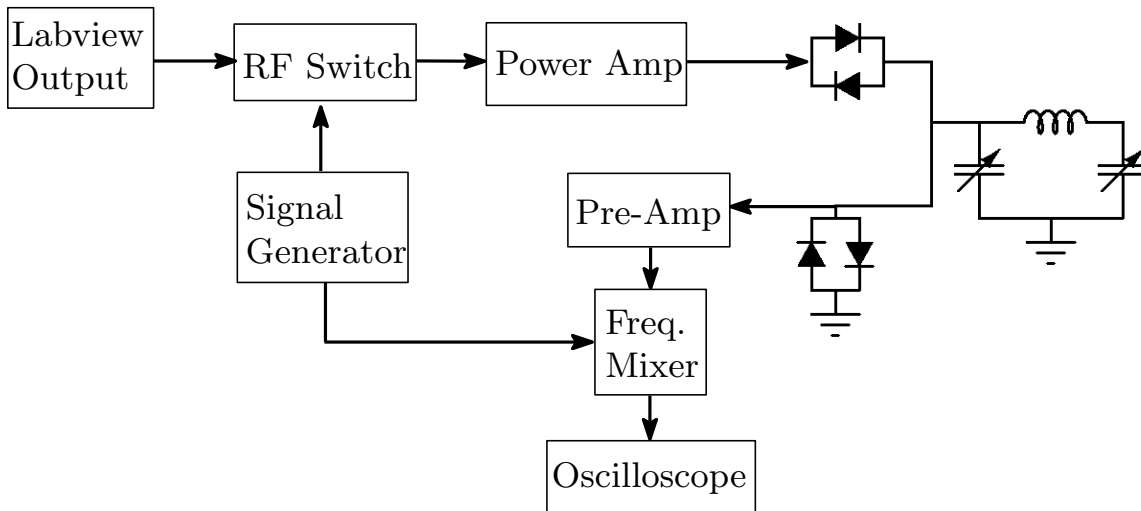


Figure 5-5: Experimental setup for finding an initial NMR signal.

5.2 Results

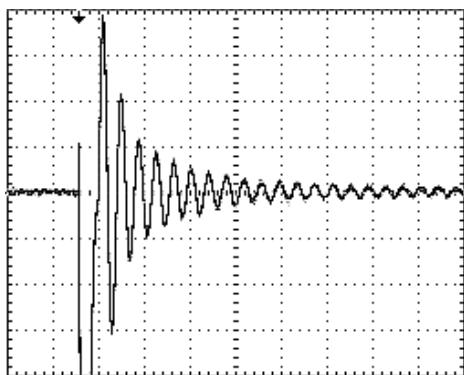
The principle result of this research was the demonstration of received NMR signals with sufficient SNR. Figure 5-6 shows analog oscilloscope shots of the observed NMR signal. Figure 5-6(a) shows the amplified received signal from the probe circuit. Figure 5-6(b) and 5-6(c) show this received signal after it was down-modulated by the frequency mixer and low-pass filtered.



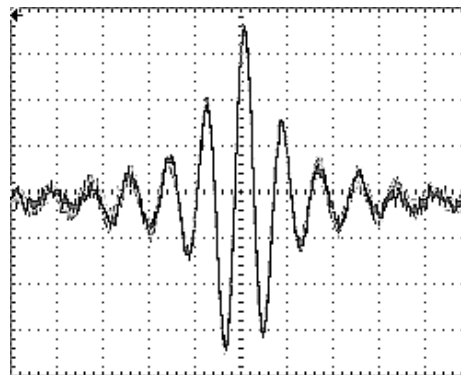
(a) Amplified NMR signal. The envelope of the FIDs and echo are clear. (b) Amplified NMR signal mixed with a sinusoid at Larmor frequency, then low-pass filtered. (c) NMR signal mixed with a sinusoid that is slightly off the Larmor frequency and filtered.

Figure 5-6: Series of oscilloscope photos that show the effect of frequency mixing the NMR signal.

Figure 5-7 shows close-ups of a Free Induction Decay (FID) curve and an Echo produced by the NMR system.



(a) Oscilloscope shot of the NMR signal, as a result of a 90° pulse. Scale: 20mV and .25ms



(b) Oscilloscope of an echo during a Spin-Echo sequence. Scale: 5mV and .25ms

Figure 5-7: Close-up shots of received FID curve and echo signal.

5.2.1 Mapping Tip Angle to Pulse Widths

In order to execute pulse sequences to measure time constants, we had to first determine the 90° and 180° pulse duration. This was done by spacing the pulses far apart and varying the pulse width while measuring the resulting FID. This was done for the preliminary magnetic structure and the improved magnetic structure. The results of this procedure are shown in figures 5-8 and 5-9.

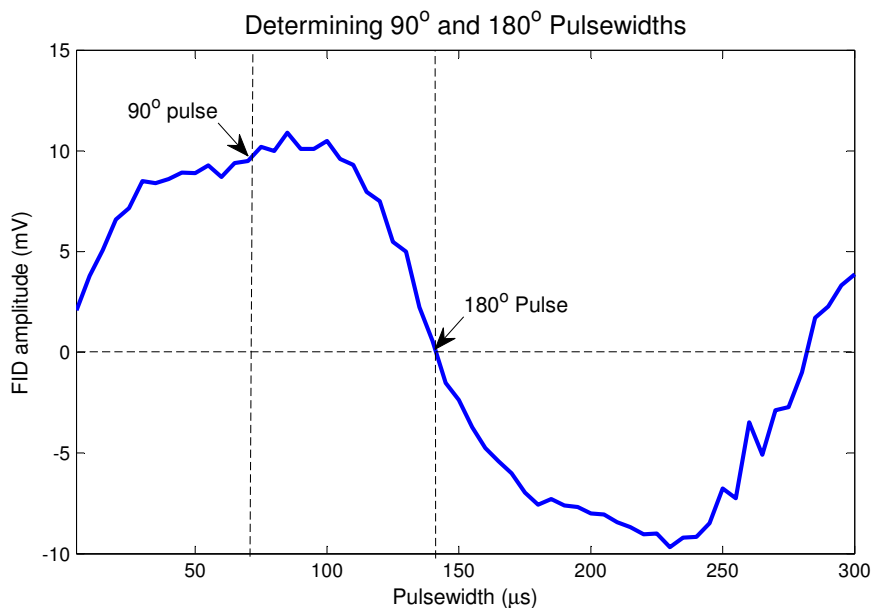


Figure 5-8: Preliminary magnetic system pulse width measurement.

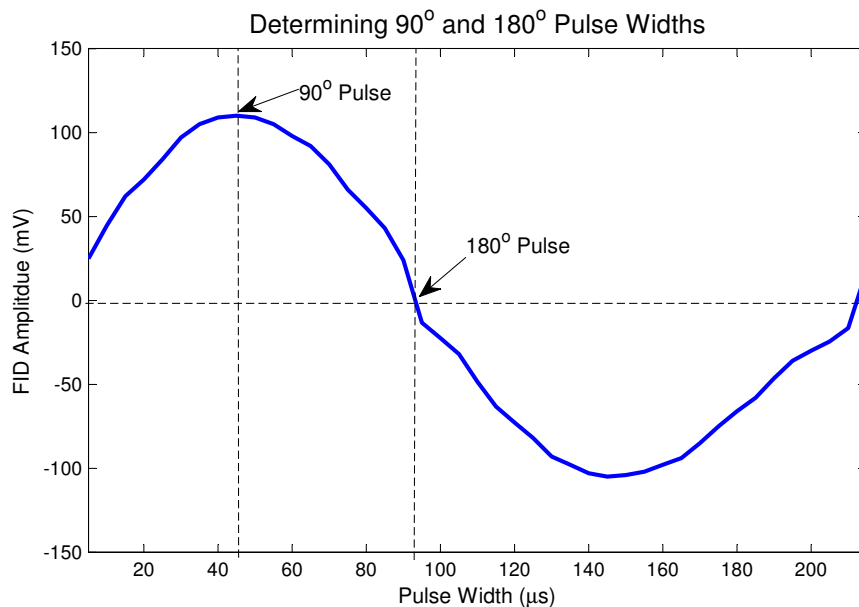


Figure 5-9: Improved magnetic system pulse width measurement.

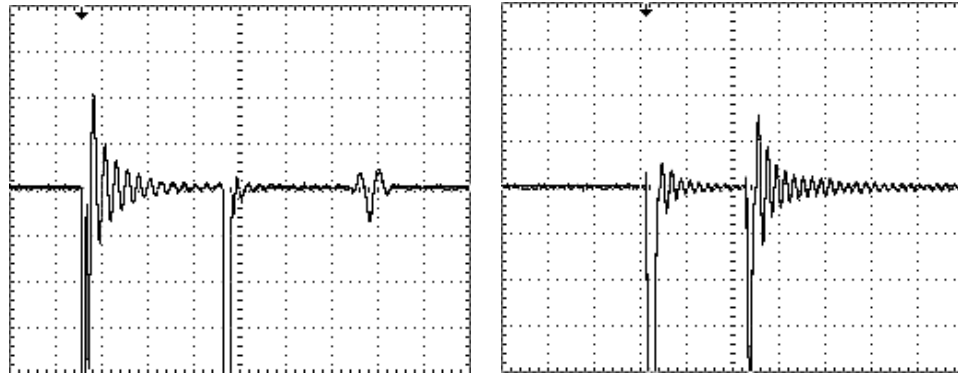
The plots in figures 5-8 and 5-9 represent the magnetization vector, \vec{M} , of the sample being rotated by the excitation field, \vec{B}_1 . The x-axis of the plots is the time duration of the pulses but also represents the tip angle, θ , of \vec{M} .

The mapping of the tip angle to pulse duration is dependant on several factors, and changing any of the variables of the experimental setup can change the mapping. For example, if the probe position is changed or the frequency or amplitude of \vec{B}_1 is changed, the duration of the 180° pulse sequence might be changed. Therefore, every time the NMR system is used it is necessary to figure out the accurate lengths of the 90° and 180° pulse widths before running an experiment. It is clear from figures 5-8 and 5-9, that data from the improved magnet system offers a higher SNR than was possible with the preliminary magnetic system (because the FID amplitude is much larger).

5.2.2 Pulse Sequence Scope Shots

After the durations of the 90° and 180° pulses were determined, we were able to execute pulse sequences used to measure time constants. Specifically the pulse sequences

used were: 90-180 (spin-echo), 180-90 (inversion-recovery), and 90-90 (another T_1 measurement sequence). Digital scope shots of a spin-echo sequence and inversion recovery sequence are shown in figures 5-10(a) and 5-10(b).



(a) Oscilloscope shot of the NMR signal, as a result of a 90-180 pulse sequence. Scale: 20mV and 1ms
 (b) Oscilloscope shot of the NMR signal, as a result of a 180-90 pulse sequence. Scale: 50mV and .5ms

Figure 5-10: Oscilloscope shots of pulse sequences.

5.2.3 Time Constant Measurement

The pulse sequences shown in figures 5-10(a) and 5-10(b) can of course be used to measure the relaxation time constants, T_2 and T_1 . T_2^* can also be measured with a single pulse.

Figure 5-11 shows the estimated shape of the T_2^* decay. This is ‘estimated’ because a portion of the FID directly after the pulse is not visible because of the ‘dead-time’ after the pulse (described in section 4.3). However, the T_2^* time constant can easily be measure from the FID. The measured time constant was $T_2^* = 98\mu s$.

T_2 measurements were done with the spin-echo sequence. Figures 5-13 and 5-12 show the result of measurements. T_2 was determined in the following way:

- The 90° and 180° pulse widths were determined and produced by either the LabVIEW program or the FPGA.
- The spacing between the two pulses, τ , was initially set to 1ms. The repeat time of the pulse was set to be much larger, around 200ms, to ensure that the sets of pulses did not effect each other.

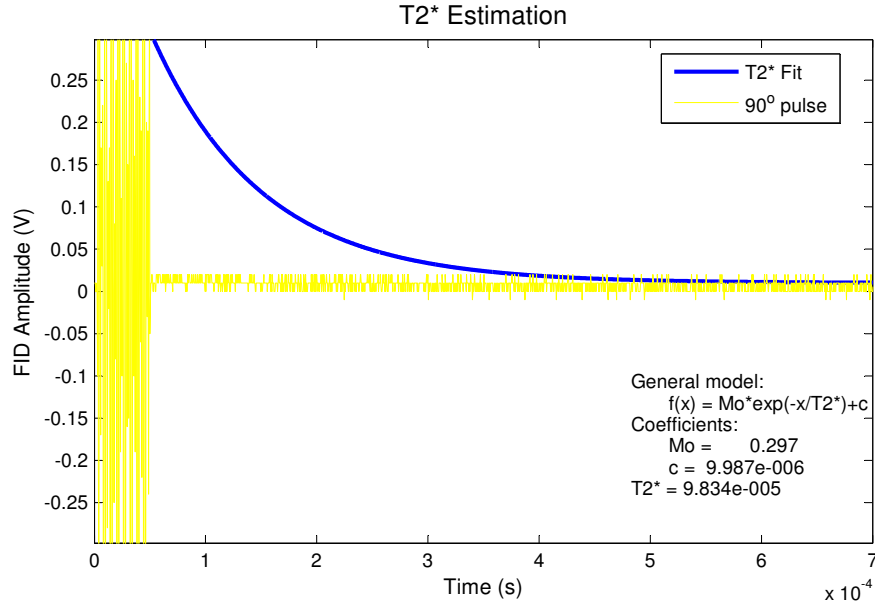


Figure 5-11: T_2^* plot

- The amplitude of the echo, which occurs at time 2τ after the first pulse, was recorded.
- τ was increased by 1ms increments while recording the echo amplitude. This was done until the echo was too small to measure, which happens much sooner for the preliminary magnetic system.
- MATLAB was used to fit a curve to the data to determine the time constant, T_2 . The data is of the form: $M_{xy}(t) = M_0 e^{-t/T_2}$

From the two data sets shown in fig. 5-12 and 5-13, T_2 was determined to be about 10ms. The data from the improved magnetic system was much easier to record, and it was possible to record more data points before the echo was too small to measure.

T_1 measurements were done with the inversion recovery sequence and the 90-90 pulse sequence. Figure 5-14 shows longitudinal relaxation data using the 90-90 pulse sequence on the preliminary magnetic system, and figure 5-15 shows data taken by applying the inversion recovery sequence to the improved magnetic system. T_1 was determined similarly to the determination of T_2 :

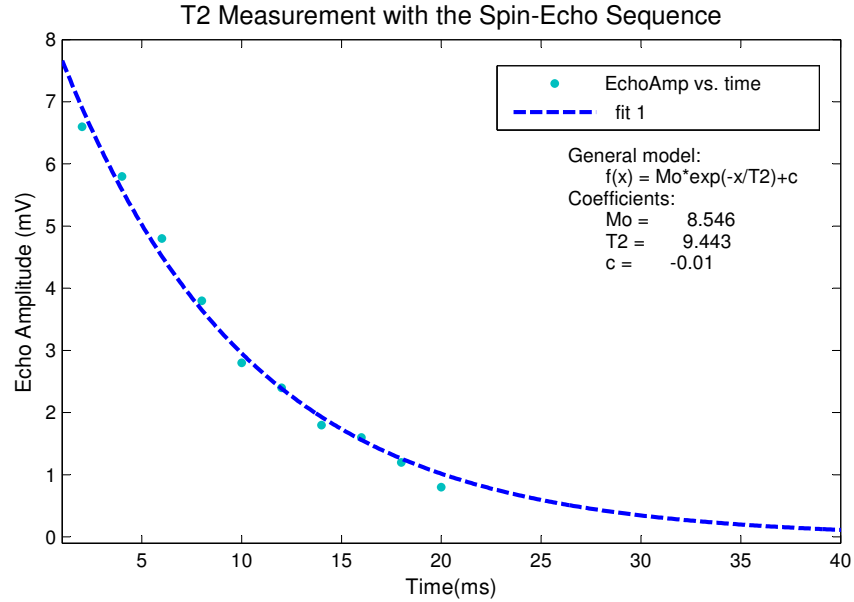


Figure 5-12: Preliminary magnetic system T_2 data.

- The pulsewidths were determined and produced by either the LabVIEW program or the FPGA.
- The spacing between the two pulses, τ , was initially set to 1ms, and the spacing between the pulses was set to be much longer.
- The amplitude of the FID, which occurs directly after the second pulse was recorded.
- τ was increased by 1ms increments while recording the FID amplitude. This was done until it was clear that curve had flattened, which means that M_z had completely recovered.
- MATLAB was used to fit a curve to the data to determine the time constant, T_1 . The data is of the form: $M_z = M_{eq} - 2M_{eq}e^{-t/T1}$ for the inversion recovery sequence, and $M_z = M_{eq} - M_{eq}e^{-t/T1}$ for the 90-90 sequence.

From the two data sets shown in fig. 5-14 and 5-15, T_1 was determined to be 15.8ms with the improved magnetic system data and 15.44ms with the preliminary magnetic system data.

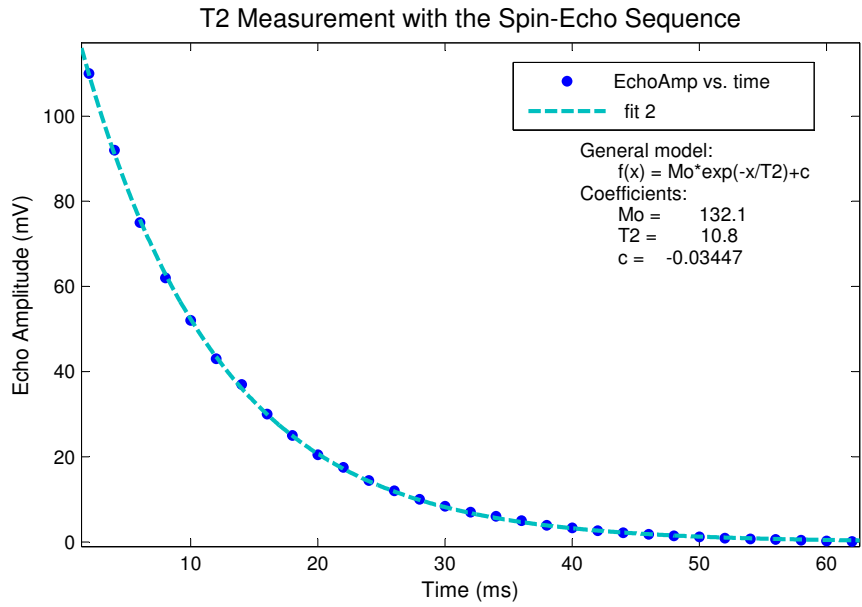


Figure 5-13: Improved magnetic system T_2 data.

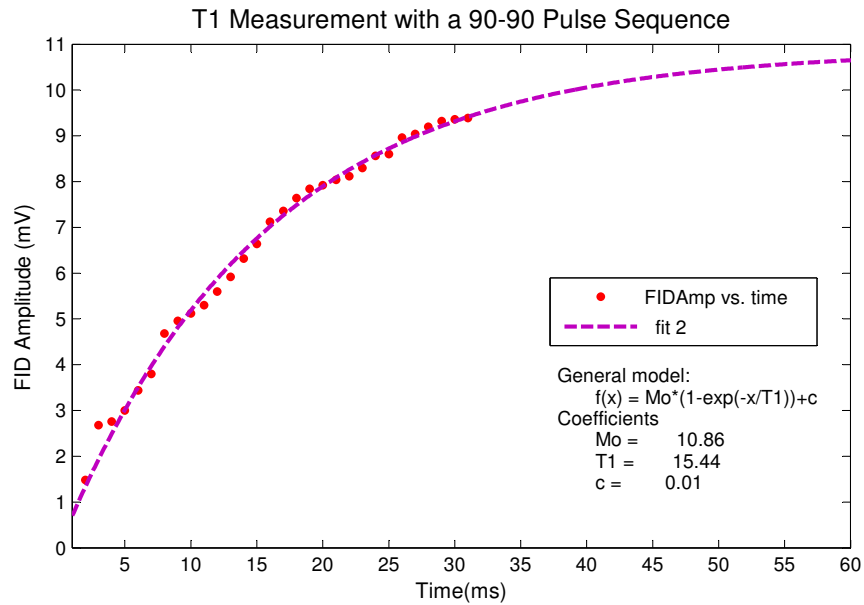


Figure 5-14: Preliminary magnetic system T_1 data.

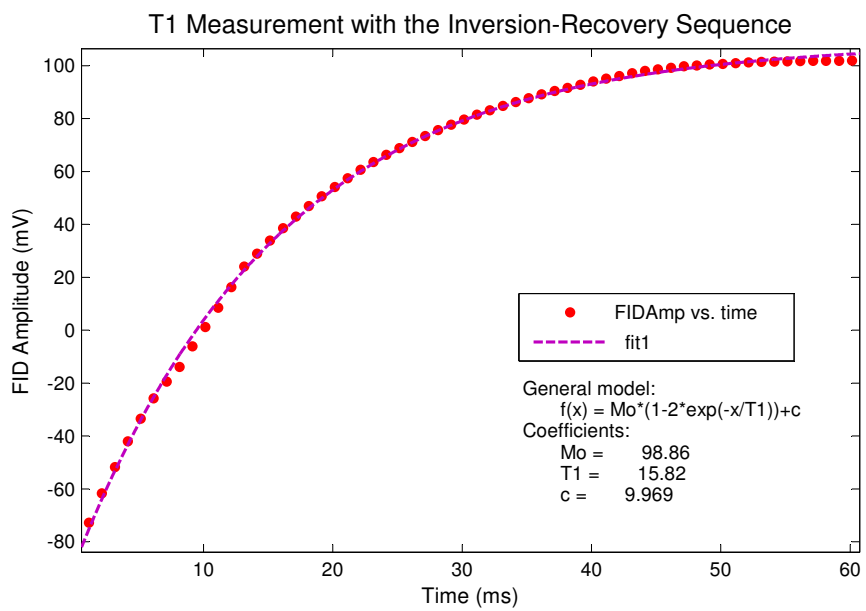


Figure 5-15: Improved magnetic system T_1 data.

Chapter 6

Conclusion

A functional low-field pulsed nuclear magnetic resonance (NMR) system for benchtop undergraduate laboratory studies was demonstrated. NMR technology and research is currently prominent, and its functionality will only continue to grow. The developed system will be a useful NMR learning tool for students. Fundamental NMR concepts that are difficult to visualize will be easily demonstrated with this system.

Although the overall analog system design is similar to traditional NMR systems, the use of the FPGA to produce pulses and process the received NMR signal was an original concept that provides broad flexibility. The FPGA can be used to easily produce complex pulse sequences, and will also be used to drive gradient coils in the future development of this system.

The use of a permanent magnet structure for establishing the static homogeneous magnetic field (\vec{B}_0) works well for this application. There were initial doubts about the safety of having a large magnetic structure in a laboratory, but this is a non-issue because the field is well contained in the sturdy permanent structure.

The preliminary magnetic structure was a great learning tool for the project design. Limitations of the design were discovered with the preliminary magnetic structure, such as the need for more amplification and shielding and the need for a more mechanically structured probe-holder. These issues were addressed in the design of the improved system. The improved system increased the signal to noise ratio (SNR) dramatically. As the results show, the amplitude of the NMR signal was increased

by almost an order of magnitude using the improved magnetic structure.

The development of the coil and probe circuit led to some interesting realizations, such as the trade-off in the resonant circuit's quality factor (Q). We want a large Q to increase signal-to-noise ratio, but we also need to avoid receiver 'dead-time' which results from pre-amp paralysis and the resonant circuit's ring-down. This requirement forces us to decrease Q .

The design of the probe holder was much more important than expected. The stability of the coil in the holder and the shielding of the coil and probe circuit were crucial, as was the ability to adjust the position of the probe easily. The mechanical design of the probe holder is neat, rigid, and allows smooth mechanical adjustments. It was a great general improvement to the useability of the system.

Finding the initial NMR signals was difficult, but once they were found it was not difficult to make adjustments to improve the SNR. The tip angle and time constant measurements fit the theoretical expectations, and the data sets are consistent.

There are a few limitations to the developed system. Although the use of the frequency mixer and low-pass filter greatly improve the SNR of the received signal, it changes the appearance of the NMR signal. When \vec{B}_1 is set to be exactly at the Larmor frequency, the output of the receiver is the envelope of the signal which does not clearly show the precession of the of atoms. When \vec{B}_1 is set to be off-resonance, the output signal exhibits oscillation which is more intuitive. However, it was very difficult to produce a perfect 180° pulse when B_1 was off resonance. This is shown in figures 5-10(a) and 5-10(b), where there is a small FID after the 180° pulse. There should not be an FID after a perfect 180° pulse because there should be no M_{xy} component of \vec{M} .

Another limitation of the system is its hydrogen specificity. The adjustability of tuning and matching capacitors is too small to allow for excitation and observation other nuclei.

This NMR system will be further developed. One topic of future work is the further improvement of the system's SNR. It is believed that this can be done with the addition of a bandpass filter, more amplification, and a Q -spoiler circuit to decouple

the need for high Q with the need for fast ring-down. While the addition of a band-pass filter and amplification is self explanatory, the addition of a Q-spoiler is more complicated. The idea is to increase the damping of the probe circuit directly after the \vec{B}_1 pulse so that power is quickly dissipated and the ring-down time is decreased. The difficult part about this additional circuitry is ensuring that it does not effect the received NMR signal.

Work is currently being done to further the use of the FPGA. Ethernet connectivity is being developed so that the received and transmitted signals can be easily observed and manipulated with a computer.

The most significant topic of further work, is the addition of gradient fields to the system. The addition of gradient coils is currently in development, and will allow positional detection of the sample. The goal is to eventually develop the NMR system into a classroom MRI system.

In the near future, a single gradient coil will be added to enable a simple experiment. In addition to \vec{B}_0 , the gradient coil will create an approximately linearly varying field in the \hat{z} direction. This varying field will create a resonant frequency gradient in the \hat{z} direction of the sample. The sample will consist of two fish oil tablets spaced about 1cm apart in the \hat{z} direction. These two tablets should produce NMR signals at slightly different frequencies. The fourier transform will be taken of the received data, which should show two close resonant peaks for the two tablets.

Appendix A

Software

A.1 LabVIEW pulse generator

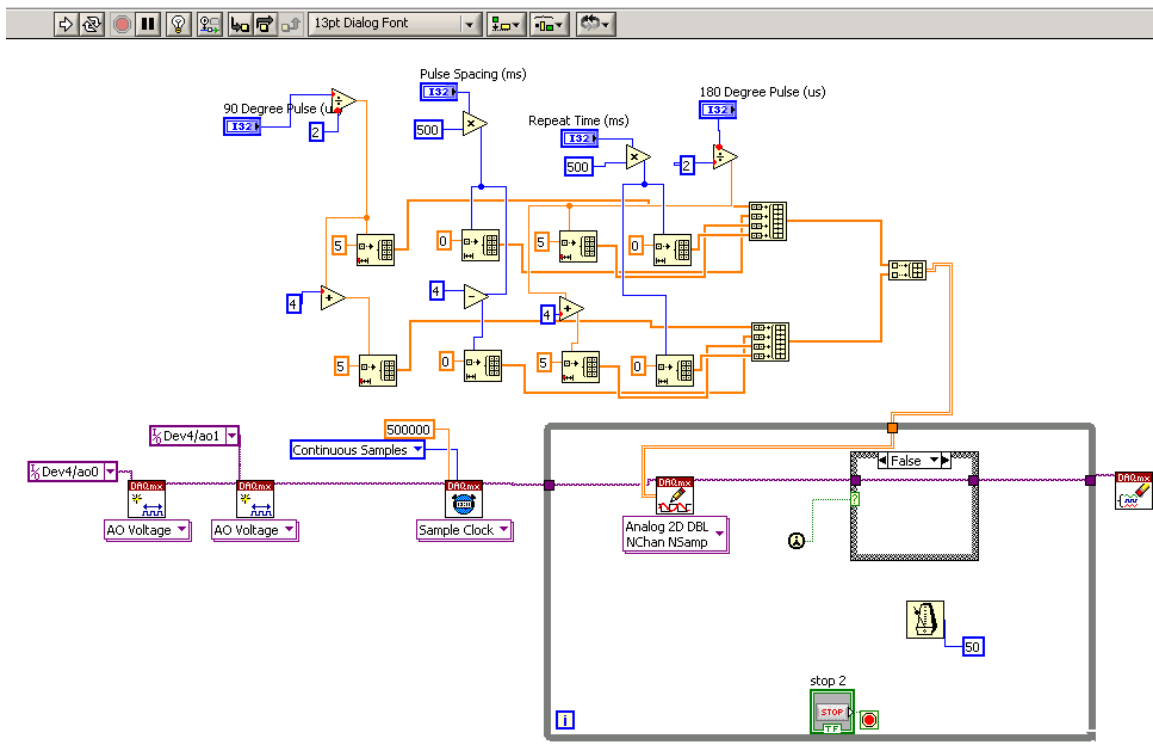


Figure A-1: LabVIEW block diagram of the pulse generation program.

A.2 FPGA Verilog code

A.2.1 top level

```
// Top Level Module for NMR signal generator and processor
// works with Altera DSP dev kit (3C120 board with analog HSMC card)

// 'define SMA_CLOCK_OUTPUT
'define USER_LEDS
// 'define HSMA
// 'define HSMB
'define LCD
// 'define DDR
// 'define SRAM
// 'define FLASH
'define ADC
'define DAC
// 'define HSMC_B

module Cephalopoda (
    // clocks and resets
        clk_50 ,
        clk_125 ,

        clk_sma ,
        clkout_sma ,

        user_resetn ,

    // User I/O
        // buttons , switches , and LEDs
        user_pb ,                // user pushbuttons
        user_dipsw ,            // user input dipsw
        user_led ,              // user LEDs

        // HSMC LEDs
        hsma_tx_led ,
        hsma_rx_led ,
        hsmb_tx_led ,
        hsmb_rx_led ,

        // Seven segment display
        seven_seg_a ,
        seven_seg_b ,
```

```

seven_seg_c ,
seven_seg_d ,
seven_seg_e ,
seven_seg_f ,
seven_seg_g ,
seven_seg_dp ,
seven_seg_sel ,

// LCD
lcd_data ,
lcd_e_rdn ,
lcd_en ,
lcd_rstn ,
lcd_wen ,
lcd_d.cn ,

// Communications Ports & Interfaces

// USB
usb_ifclk ,
//usb_cmd_data
//usb_empty
//usb_fd
//usb_full
//usb_ifclk
//usb_ifclk
//usb_ren
//usb_wen

// ethernet
enet_rx_clk ,

// memory
// DDR
ddr2bot_a ,
ddr2bot_ba ,
ddr2bot_casn ,
ddr2bot_cke ,
ddr2_ck_n ,
ddr2_ck_p ,
ddr2bot_csn ,
ddr2_dm ,
ddr2_dq ,
ddr2_dqs ,
ddr2bot_rasn ,

```

```

    ddr2bot_wen ,
    ddr2bot_odt ,

    // SRAM
    sram_ben ,
    sram_clk ,
    sram_csn ,
    sram_oen ,
    sram_psn ,
    sram_wait ,
    sram_wen ,
    sram_advn ,

    // FSM bus (shared between SRAM, flash , and MAX II)
    fsa ,
    fsd ,

    // flash
    flash_oen ,
    flash_cen ,
    flash_wen ,
    flash_resetn ,

// data conversion HSMC card
    // ADC
    adc_sclk ,
    adc_sdata ,
    ada_oe ,
    ada_dco ,
    ada_d ,
    ada_or ,
    ada_cs ,
    adb_oe ,
    adb_dco ,
    adb_d ,
    adb_or ,
    adb_cs ,

    //DAC
    pclk0 ,
    da ,
    data bus for DAC A
    db ,
    data bus for DAC B
    // DAC clock
    //
    //

```

```

// HSMC port B
// HSMC
pclk1 ,

//          hsmb_clk_in_p ,
//          hsmb_clk_in_n ,
hsmb_clk_out_p ,
hsmb_clk_out_n
);

// clocks and resets
input      clkin_50;
input      clkin_125;

input      clkin_sma;
output     clkout_sma;

input      user_resetcn;

`ifndef SMA_CLOCK_OUTPUT
    assign clkout_sma = 1'b z;
`endif

// User I/O
// buttons, switches, and LEDs
input  [7:0]  user_dipsw;    //1.8V          user input dipsw
output [7:0]  user_led;     //LVTTL        user LEDs
input  [3:0]  user_pb;      //1.8V          user pushbuttons

`ifndef USER_LEDS
    assign user_led = { user_pb, user_pb };
`endif

// HSMC LEDs
output     hsma_tx_led;
output     hsma_rx_led;
output     hsmb_tx_led;
output     hsmb_rx_led;

`ifndef HSMA
    assign hsma_tx_led = 0;
    assign hsma_rx_led = 0;
`endif

`ifndef HSMB

```

```

        assign hsmb_tx_led = 0;
        assign hsmb_rx_led = 0;
    'endif

    // Seven segment display
    output          seven_seg_a;          //LVTTL
    output          seven_seg_b;          //LVTTL
    output          seven_seg_c;          //LVTTL
    output          seven_seg_d;          //LVTTL
    output          seven_seg_e;          //LVTTL
    output          seven_seg_f;          //LVTTL
    output          seven_seg_g;          //LVTTL
    output          seven_seg_dp;         //LVTTL
    output [4:1]    seven_seg_sel;        //LVTTL

    wire [6:0] seven_seg;

    assign {
        seven_seg_a , seven_seg_b , seven_seg_c ,
        seven_seg_d , seven_seg_e , seven_seg_f ,
        seven_seg_g } = seven_seg;

    'ifndef SEVEN_SEGMENT
        assign seven_seg = ~7'b 1110111;
        assign seven_seg_sel = 4'b1111;
        assign seven_seg_dp = 1'b1;
    'endif

    // LCD
    output [7:0]    lcd_data;
    output          lcd_e_rdn;
    output          lcd_en;
    output          lcd_rstn;
    output          lcd_wen;
    output          lcd_d_cn;

    'ifndef LCD
        assign lcd_data = 8'b 0;
        assign lcd_e_rdn = 1'b 1;
        assign lcd_en = 1'b 1;
        assign lcd_rstn = 1'b 1;
        assign lcd_wen = 1'b 1;
        assign lcd_d_cn = 1'b 1;
    'endif

```

// Communications Ports & Interfaces

```

// USB
input                usb_ifclk ;
//                  usb_cmd_data
//                  usb_empty
//                  usb_fd
//                  usb_full
//                  usb_ifclk
//                  usb_ifclk
//                  usb_ren
//                  usb_wen

// Ethernet
input                enet_rx_clk ;

// Memory
// DDR
output [ 12: 0 ] ddr2bot_a ;
output [  1: 0 ] ddr2bot_ba ;
output                ddr2bot_casn ;
output                ddr2bot_cke ;
output                ddr2bot_odt ;
inout  [  2: 0 ] ddr2_ck_n ;
inout  [  2: 0 ] ddr2_ck_p ;
output                ddr2bot_csn ;
output [  1: 0 ] ddr2_dm ;
inout  [ 71: 0 ] ddr2_dq ;
inout  [  1: 0 ] ddr2_dqs ;
output                ddr2bot_rasn ;
output                ddr2bot_wen ;

`ifndef DDR
    assign ddr2bot_a = 13'b zzzzzzzzzzzzz ;
    assign ddr2bot_ba = 2'b z ;
    assign ddr2bot_casn = 1'b z ;
    assign ddr2bot_cke = 1'b z ;
    assign ddr2bot_odt = 1'b z ;
    assign ddr2_ck_n = 3'b zzz ;
    assign ddr2_ck_p = 3'b zzz ;
    assign ddr2bot_csn = 1'b z ;
    assign ddr2_dm = 2'b z ;
    assign ddr2_dq = 72'h zzzzzzzzzzzzzzzzzzz ;
    assign ddr2_dqs = 1'b z ;
    assign ddr2bot_rasn = 1'b z ;
    assign ddr2bot_wen = 1'b z ;
`endif

```



```

// data conversion HSMC card
// ADC
output          adc_sclk;          //XXXXXX; LVTTL  (serial port
                                interface clock, serial port mode)
input           adc_sdata;         //XXXXXX; LVTTL  (serial port
                                interface data inout/output, serial port mode)
output          ada_oe;            //XXXXXX; LVTTL  (output enable,
                                active low)
input           ada_dco;           //Bank4; 1.8V   fpga clk input (data
                                clock output)
input [13:0]    ada_d;             //Bank4; 1.8V   (data output)
input           ada_or;            //Bank4; 1.8V   (out of range
                                indicator)
output          ada_cs;            //XXXXXX; LVTTL  (serial port
                                interface chip select, active low)

output          adb_oe;            //XXXXXX; LVTTL
input           adb_dco;           //Bank4; 1.8V   fpga clk input
input [13:0]    adb_d;             //Bank4; 1.8V
input           adb_or;            //Bank4; 1.8V
output          adb_cs;            //XXXXXX; LVTTL

`ifndef ADC
    assign adc_sclk = 1'b 1;
    assign adc_sdata = 1'b z;
    assign ada_oe = 1'b 1;
    assign ada_cs = 1'b 1;
    assign adb_oe = 1'b 1;
    assign adb_cs = 1'b 1;
`endif

//DAC
output          pclk0;
output [13:0]   da;
output [13:0]   db;

`ifndef DAC
    assign pclk0 = 1'b 1;
    assign da = 14'h 0000;
    assign db = 14'h 0000;
`endif

// HSMC port B
// clocks
output          pclk1;

```

```

// HSMC Port B
    //      input [1:2]          hsmb_clk_in_p;
    //      input [1:2]          hsmb_clk_in_n;
    output [1:2]          hsmb_clk_out_p;
    output [1:2]          hsmb_clk_out_n;

// ----- wires -----

// clocks and resets
wire clk;

// NCO outputs
wire signed [13:0] signal1;
wire signed [13:0] signal2;

// signal gate outputs
//wire gate;
wire [13:0] gate1;
wire gate;
wire trigger;

// window function generator outputs
wire [12:0] windowAmplitude;

// configuration register outputs
wire [31:0] phaseIncrement;
wire [31:0] pulse90ActiveTicks;
wire [31:0] pulse90InactiveTicks;
wire [31:0] pulse180ActiveTicks;
wire [31:0] pulse180InactiveTicks;

//freq multiplier output
wire signed [13:0] demodsigned;
wire [13:0] demodunsigned;

//fir output
wire [13:0] filteredunsigned;
wire signed [13:0] filteredsigned;

//ADC inputs
wire [13:0] analogsig_a;
wire [13:0] analogsig_b;

```

```

// ----- module instances -----
assign analogsig_a = ada_d;
assign analogsig_b = adb_d;

SystemClockPll pll_inst (
    .inclk0 (clk_in_50),
    .c0 (clk)
);

SignalGate      SignalGate_inst(
    .Gate(gate),
    .Gate1(gate1),
    .Trigger(trigger),
    .Pulse90ActiveTicks(pulse90ActiveTicks),
    .Pulse90InactiveTicks(pulse90InactiveTicks),
    .Pulse180ActiveTicks(pulse180ActiveTicks),
    .Pulse180InactiveTicks(pulse180InactiveTicks),
    .Reset_n(user_resetn),
    .Clock(clk)
);

WindowFunctionGenerator WindowFunctionGenerator_inst(
    .WindowOutput(windowAmplitude),
    .GateInput(gate),
    .Reset_n(user_resetn),
    .Clock(clk)
);

SinewaveGenerator SinewaveGenerator_inst (
    .SignalOutput(signal1),
    .Amplitude(windowAmplitude),
    .PhaseIncrement(phaseIncrement),
    .Enable(1'b 1),
    .Reset_n(user_resetn),
    .Clk(clk)
);

SinewaveGenerator SinewaveGenerator_inst2 (
    .SignalOutput(signal2),
    .Amplitude(13'h1000),
    .PhaseIncrement(phaseIncrement),

```

```

        .Enable(1'b 1),
        .Reset_n(user_resetn),
        .Clk(clk)
    );

    FrequencyMultiply FrequencyMultiply_inst (
        .MultipliedSigs(demodsigned),
        .MultipliedSigu(demodunsigned),
        .Signal1(analogsiga),
        .Signal2(signal2),
        .Clock(clk)
    );

    FIR fir_inst (
        .Y(filteredsigned),
        .Yunsign(filteredunsigned),
        .X(demodsigned),
        .b0(8'b 00000010), .b1(8'b 00000011), .b2(8'b 00000011), .b3(8'b
            00000100), .b4(8'b 00000101), .b5(8'b 00000110), .b6(8'b
            00000111), .b7(8'b 00001001), .b8(8'b 00001010), .b9(8'b
            00001100),
        .b10(8'b 00001110), .b11(8'b 00010000), .b12(8'b 00010010), .b13(8'b
            00010101), .b14(8'b 00010111), .b15(8'b 00011001), .b16(8'b
            00011011), .b17(8'b 00011101), .b18(8'b 00011110), .b19(8'b
            00100000),
        .b20(8'b 00100001), .b21(8'b 00100010), .b22(8'b 00100011), .b23(8'b
            00100100), .b24(8'b 00100100), .b25(8'b 00100100), .b26(8'b
            00100100), .b27(8'b 00100100), .b28(8'b 00100011), .b29(8'b
            00100010),
        .b30(8'b 00100001), .b31(8'b 00100000), .b32(8'b 00011110), .b33(8'b
            00011101), .b34(8'b 00011011), .b35(8'b 00011001), .b36(8'b
            00010111), .b37(8'b 00010101), .b38(8'b 00010010), .b39(8'b
            00010000),
        .b40(8'b 00001110), .b41(8'b 00001100), .b42(8'b 00001010), .b43(8'b
            00001001), .b44(8'b 00000111), .b45(8'b 00000110), .b46(8'b
            00000101), .b47(8'b 00000100), .b48(8'b 00000011), .b49(8'b
            00000011),
        .b50(8'b 00000010),
        .Clock(clk)
    );

    // configuration registers

```

```

ConfigurationRegisters ConfigurationRegisters_inst (
    .PhaseIncrement(phaseIncrement),
    .Pulse90ActiveTicks(pulse90ActiveTicks),
    .Pulse90InactiveTicks(pulse90InactiveTicks),
    .Pulse180ActiveTicks(pulse180ActiveTicks),
    .Pulse180InactiveTicks(pulse180InactiveTicks),
    .IncreaseFrequency(~user_pb[0] && ~user_dipsw[0]),
    .DecreaseFrequency(~user_pb[1] && ~user_dipsw[0]),
    .IncreasePulseWidth(~user_pb[0] && user_dipsw[0]),
    .DecreasePulseWidth(~user_pb[1] && user_dipsw[0]),
    .IncreaseTau(~user_pb[2] && user_dipsw[0]),
    .DecreaseTau(~user_pb[3] && user_dipsw[0]),
    .Reset_n(user_resetn),
    .Clk(clk) );

assign user_led = phaseIncrement[7:0];
assign lcd_data = phaseIncrement[7:0];
assign pclk1 = trigger;

// DAC output
assign pclk0 = clk;
assign da = signal1;
assign db = filteredunsigned;

```

```
endmodule
```

A.2.2 Configuration Registers

```

// Implementation of all programmable configuration registers
// Written by Steven Wasserman: initial version implemented with constant values for
// testing

module ConfigurationRegisters(
    PhaseIncrement, Pulse90ActiveTicks, Pulse90InactiveTicks, Pulse180ActiveTicks
    , Pulse180InactiveTicks,

    IncreaseFrequency, DecreaseFrequency, IncreasePulseWidth, DecreasePulseWidth,
    IncreaseTau, DecreaseTau,

    Reset_n, Clk );

output[31:0] PhaseIncrement;
output[31:0] Pulse90ActiveTicks;
output[31:0] Pulse90InactiveTicks;

```

```

output [31:0] Pulse180ActiveTicks;
output [31:0] Pulse180InactiveTicks;
input IncreaseFrequency;
input DecreaseFrequency;
input Reset_n;
input Clk;

input IncreasePulseWidth;
input DecreasePulseWidth;
input IncreaseTau;
input DecreaseTau;

reg [31:0] phaseIncrement;
reg [11:0] gate;

reg [31:0] pulse90ActiveTicks;
reg [31:0] pulse90InactiveTicks;

always @(posedge Clk)
begin
    if( IncreaseFrequency & (gate % 12 'h 80 == 0))
    begin
        phaseIncrement <= #1 phaseIncrement + 1;
    end

    if( DecreaseFrequency & (gate % 12'h 80 == 0))
    begin
        phaseIncrement <= #1 phaseIncrement - 1;
    end

    if( IncreasePulseWidth & (gate % 16 'h 4000 == 0))
    begin
        pulse90ActiveTicks <= #1 pulse90ActiveTicks + 1;
    end

    if( DecreasePulseWidth & (gate % 16'h 4000 == 0) & pulse90ActiveTicks
        > 1'b 1)
    begin
        pulse90ActiveTicks <= #1 pulse90ActiveTicks - 1;
    end

    if( IncreaseTau & (gate % 16 'h 4000 == 0))
    begin
        pulse90InactiveTicks <= #1 pulse90InactiveTicks + 1;

```

```

        end

        if( DecreaseTau & (gate % 16'h 4000 == 0) & pulse90InactiveTicks > 1'
            b 1)
        begin
            pulse90InactiveTicks <= #1 pulse90InactiveTicks - 1;
        end

        if( ~Reset_n )
        begin

            phaseIncrement <= #1 32'h 5C81A40;
            gate = 0;
            pulse90ActiveTicks <= #1 32'h 0001D4C;
            pulse90InactiveTicks <= #1 32'h 0030D40;

        end

        gate <= #1 gate + 1;

    end

    assign Pulse90ActiveTicks = pulse90ActiveTicks;
    assign Pulse90InactiveTicks = pulse90InactiveTicks;
    assign Pulse180ActiveTicks = pulse90ActiveTicks * 2;
    assign Pulse180InactiveTicks = 32'h 0989680;
    assign PhaseIncrement = phaseIncrement;
endmodule

```

A.2.3 Signal Gate

```

// Pulse Gate for NMR waveform synthesizer
// Written by Steven Wasserman

module SignalGate( Gate, Gate1, Trigger, Pulse90ActiveTicks, Pulse90InactiveTicks,
    Pulse180ActiveTicks, Pulse180InactiveTicks, Clock, Reset_n );

    output Gate;
    output [13:0] Gate1;
    output Trigger;

    input [31:0] Pulse90ActiveTicks;
    input [31:0] Pulse90InactiveTicks;
    input [31:0] Pulse180ActiveTicks;

```

```

input [31:0] Pulse180InactiveTicks;
input Clock;
input Reset_n;

parameter pulse90Active = 2'h 0;
parameter pulse90Inactive = 2'h 1;
parameter pulse180Active = 2'h 2;
parameter pulse180Inactive = 2'h 3;

reg [1:0] state;
reg [31:0] count;
reg gate;
reg trigger;

always @(posedge Clock)
begin
    trigger <= 0;
    count <= count - 1;

    case(state)
        pulse90Active :
            begin
                gate <= 1'b 1;
                trigger <= 1'b 1;
                if(count == 0)
                begin
                    count <= Pulse90InactiveTicks;
                    state <= 1;
                end
            end

        pulse90Inactive :
            begin
                gate <= 1'b 0;
                if(count == 0)
                begin
                    count <= Pulse180ActiveTicks;
                    state <= 2;
                end
            end

        pulse180Active :
            begin
                gate <= 1'b 1;

```

```

        if(count == 0)
        begin
            count <= Pulse180InactiveTicks;
            state <= 3;
        end

        end

        pulse180Inactive :
        begin
            gate <= 1'b 0;
            if(count == 0)
            begin
                count <= Pulse90ActiveTicks;
                state <= 0;
            end

            end

        endcase

        if(~Reset_n)
        begin
            state <= 0;
            count <= Pulse90ActiveTicks;
            gate <= 1'b 0;

            end

        end // of alwas @(posedge clk)

        assign Gate1 = gate*1000;
        assign Gate = gate;
        assign Trigger = trigger;

endmodule

```

A.2.4 Window Function Generator

```

//Wavefunction Generator, produces smooth pulses.
// Written by Steven Wasserman

module WindowFunctionGenerator( WindowOutput, GateInput, Reset_n, Clock);

    output [12:0] WindowOutput;

    input GateInput;

```

```

input Reset_n;
input Clock;

reg [4:0] count;

always @(posedge Clock)
begin
    if (GateInput & (count != 5'h 1F))
    begin
        count <= count + 5'h 1;
    end

    if (~GateInput & (count != 5'h 0))
    begin
        count <= count - 5'h 1;
    end

    if (~Reset_n)
    begin
        count <= 0;
    end

end

// ROM instance
WindowFunctionRom WindowFunctionRom_inst(
    .address(count),
    .clock(Clock),
    .q(WindowOutput)
);
endmodule

```

A.2.5 Sinewave Generator

```

// Sinewave Generator for NMR signal generator
// includes quarter-wave sin ROM, amplitude modulation, and enable inputs
// Written by Steven Wasserman

module SinewaveGenerator ( SignalOutput, Amplitude, PhaseIncrement, Enable, Reset_n,
    Clk );

output [13:0] SignalOutput;
    // 14-bit unsigned output

```

```

input [12:0] Amplitude;
                // 13-bit unsigned input; max value: 13'h 1000
input [31:0] PhaseIncrement;
input Enable;
                // phase stays constant when disabled
input Reset_n;
input Clk;

reg [14:0] sinRomAddress;
reg [31:0] phaseCount, zphaseCount, z2phaseCount, z3phaseCount, z4phaseCount;
reg [24:0] scaledMagnitude;
reg [14:0] signalOutput;
// reg [15:0] sig;
// reg [15:0] signalshifted;

wire [13:0] romOutput;

always@(posedge Clk)
begin
    if(Enable)
                                // maintain current phase if not enabled
        begin
            phaseCount <= #1 phaseCount + PhaseIncrement;
        end

    if(~Reset_n)
                                // set phase count to 0 on reset
        begin
            phaseCount <= #1 32'h 0;
        end

    // create delayed versions of phaseCount value
    zphaseCount <= #1 phaseCount;
    z2phaseCount <= #1 zphaseCount;
    z3phaseCount <= #1 z2phaseCount;
    z4phaseCount <= #1 z3phaseCount;

    // compute ROM address corresponding to current phase count
    // run through the ROM forward of 0-pi/2 and
    sinRomAddress <= #1 (~phaseCount[30]) ? phaseCount[29:15] : ~phaseCount
        [29:15];

    // ROM output is delayed 2 pipeline stages delayed from phaseCount

    // apply scale factor to output

```

```

scaledMagnitude <= #1 romOutput[13:1] * Amplitude;

// scaledMagnitude is three pipeline stages delayed from phaseCount

// compute final output value:
//     offset by half scale (15'h 8000) for unsigned result
//     add ROM output for 0 - pi/4 and pi/2 - 3 * pi/2; subtract otherwise
signalOutput <= #1 (~z4phaseCount[31]) ? { 1'b 1, scaledMagnitude[24:11]} :
    {1'b 0, 14'h 3FFF - scaledMagnitude[24:11] };

// signalOutput is four pipeline stages delayed from phaseCount

end

assign SignalOutput = signalOutput[14:1];

// ROM instance — contains one quarter of a sine function

RomSin15x14 RomSin_inst (
    .address(sinRomAddress),
    .clock(Clk),
    .q(romOutput));

endmodule

```

A.2.6 Frequency Multiplier

```

// Frequency Multiplier for NMR
// written by Clarissa Zimmerman

module FrequencyMultiply( MultipliedSigs, MultipliedSigu, Signal1, Signal2, Clock );

    output signed[13:0] MultipliedSigs;
    output [13:0] MultipliedSigu;
    input [13:0] Signal1;
    input [13:0] Signal2;
    input Clock;

    //reg signed[27:0] sig1, sig2;
    reg signed[27:0] multipliedSig;
    reg signed[14:0] sig1signed, sig2signed, sig1shifted, sig2shifted;
    reg [13:0] multipliedSigshifted;

```

```

    reg signed [13:0] multipliedSigsigned;

//assign Signal1 = sig1;
//assign Signal2 = sig2;

assign MultipliedSigs = multipliedSigsigned;
assign MultipliedSigu = multipliedSigshifted;

    always @(posedge Clock)
    begin
        sig1signed <= $signed({1'b0,Signal1});
        sig2signed <= $signed({1'b0,Signal2});
        sig1shifted <= sig1signed - 14'h2000;
        sig2shifted <= sig2signed - 14'h2000;
        multipliedSig <= (sig1shifted *2) * sig2shifted;
        multipliedSigshifted <= multipliedSig[26:13] +14'h2000;
        multipliedSigsigned <= $signed(multipliedSig[26:13]);
    end // of always @(posedge clk)

endmodule

```

A.2.7 FIR Filter

```

// Low pass filter for NMR
// written by Clarissa Zimmerman

module FIR( Y, Yunsign, X, b0, b1, b2, b3, b4, b5, b6, b7, b8, b9, b10, b11, b12, b13
    , b14, b15, b16, b17, b18, b19, b20, b21, b22, b23, b24, b25, b26, b27, b28, b29,
    b30, b31, b32, b33, b34, b35, b36, b37, b38, b39, b40, b41, b42, b43, b44, b45,
    b46, b47, b48, b49, b50, Clock );

output signed [13:0] Y;
output [13:0] Yunsign;
input signed [13:0] X;
input signed [7:0] b0, b1, b2, b3, b4, b5, b6, b7, b8, b9, b10, b11, b12, b13, b14,
    b15, b16, b17, b18, b19, b20, b21, b22, b23, b24, b25, b26, b27, b28, b29, b30,
    b31, b32, b33, b34, b35, b36, b37, b38, b39, b40, b41, b42, b43, b44, b45, b46,
    b47, b48, b49, b50;
input Clock;

reg signed [13:0] X0, X1, X2, X3, X4, X5, X6, X7, X8, X9, X10, X11, X12, X13, X14, X15
    , X16, X17, X18, X19, X20, X21, X22, X23, X24, X25, X26, X27, X28, X29, X30, X31,

```

```

    X32, X33, X34, X35, X36, X37, X38, X39, X40, X41, X42, X43, X44, X45, X46, X47,
    X48, X49, X50;

reg signed [21:0] prod0, prod1, prod2, prod3, prod4, prod5, prod6, prod7, prod8, prod9
, prod10, prod11, prod12, prod13, prod14, prod15, prod16, prod17, prod18, prod19
, prod20, prod21, prod22, prod23, prod24, prod25, prod26, prod27, prod28, prod29,
prod30, prod31, prod32, prod33, prod34, prod35, prod36, prod37, prod38, prod39,
prod40, prod41, prod42, prod43, prod44, prod45, prod46, prod47, prod48, prod49,
prod50;
reg signed [13:0] Prod0, Prod1, Prod2, Prod3, Prod4, Prod5, Prod6, Prod7, Prod8, Prod9
, Prod10, Prod11, Prod12, Prod13, Prod14, Prod15, Prod16, Prod17, Prod18, Prod19
, Prod20, Prod21, Prod22, Prod23, Prod24, Prod25, Prod26, Prod27, Prod28, Prod29,
Prod30, Prod31, Prod32, Prod33, Prod34, Prod35, Prod36, Prod37, Prod38, Prod39,
Prod40, Prod41, Prod42, Prod43, Prod44, Prod45, Prod46, Prod47, Prod48, Prod49,
Prod50;
reg signed [14:0] add1, add2, add3, add4, add5, add6, add7, add1b, add2b, add3b, add4b
, add5b, add6b, add7b;
reg signed [15:0] addtotal1, addtotal2, addtotal3, addtotal4;
reg signed [16:0] addfinal;
reg signed [20:0] addtrunc1;
reg signed [13:0] yout,y;
reg [13:0] yunsign;

assign Y = y;
assign Yunsign = yunsign;

always @(posedge Clock) begin

    X50 <=X49;
    X49 <= X48;
    X48 <= X47;
    X47 <= X46;
    X46 <= X45;
    X45 <= X44;
    X44 <= X43;
    X43 <= X42;
    X42 <= X41;
    X41 <= X40;
    X40 <=X39;
    X39 <= X38;
    X38 <= X37;
    X37 <= X36;
    X36 <= X35;
    X35 <= X34;
    X34 <= X33;

```

```
X33 <= X32;
X32 <= X31;
X31 <= X30;
X30 <= X29;
X29 <= X28;
X28 <= X27;
X27 <= X26;
X26 <= X25;
X25 <= X24;
X24 <= X23;
X23 <= X22;
X22 <= X21;
X21 <= X20;
X20 <=X19;
X19 <= X18;
X18 <= X17;
X17 <= X16;
X16 <= X15;
X15 <= X14;
X14 <= X13;
X13 <= X12;
X12 <= X11;
X11 <= X10;
X10 <=X9;
X9 <= X8;
X8 <= X7;
X7 <= X6;
X6 <= X5;
X5 <= X4;
X4 <= X3;
X3 <= X2;
X2 <= X1;
X1 <= X0;
X0 <= X;

prod0 <= X0 * b0;
prod1 <= X1 * b1;
prod2 <= X2 * b2;
prod3 <= X3 * b3;
prod4 <= X4 * b4;
prod5 <= X5 * b5;
prod6 <= X6 * b6;
prod7 <= X7 * b7;
prod8 <= X8 * b8;
prod9 <= X9 * b9;
```

prod10 <= X10 * b10;

prod11 <= X11 * b11;

prod12 <= X12 * b12;

prod13 <= X13 * b13;

prod14 <= X14 * b14;

prod15 <= X15 * b15;

prod16 <= X16 * b16;

prod17 <= X17 * b17;

prod18 <= X18 * b18;

prod19 <= X19 * b19;

prod20 <= X20 * b20;

prod21 <= X21 * b21;

prod22 <= X22 * b22;

prod23 <= X23 * b23;

prod24 <= X24 * b24;

prod25 <= X25 * b25;

prod26 <= X26 * b26;

prod27 <= X27 * b27;

prod28 <= X28 * b28;

prod29 <= X29 * b29;

prod30 <= X30 * b30;

prod31 <= X31 * b31;

prod32 <= X32 * b32;

prod33 <= X33 * b33;

prod34 <= X34 * b34;

prod35 <= X35 * b35;

prod36 <= X36 * b36;

prod37 <= X37 * b37;

prod38 <= X38 * b38;

prod39 <= X39 * b39;

prod40 <= X40 * b40;

prod41 <= X41 * b41;

prod42 <= X42 * b42;

prod43 <= X43 * b43;

prod44 <= X44 * b44;

prod45 <= X45 * b45;

prod46 <= X46 * b46;

prod47 <= X47 * b47;

prod48 <= X48 * b48;

prod49 <= X49 * b49;

prod50 <= X50 * b50;

```
Prod0 <= prod0 [21:8];
Prod1 <= prod1 [21:8];
Prod2 <= prod2 [21:8];
Prod3 <= prod3 [21:8];
Prod4 <= prod4 [21:8];
Prod5 <= prod5 [21:8];
Prod6 <= prod6 [21:8];
Prod7 <= prod7 [21:8];
Prod8 <= prod8 [21:8];
Prod9 <= prod9 [21:8];
Prod10 <= prod10 [21:8];
Prod11 <= prod11 [21:8];
Prod12 <= prod12 [21:8];
Prod13 <= prod13 [21:8];
Prod14 <= prod14 [21:8];
Prod15 <= prod15 [21:8];
Prod16 <= prod16 [21:8];
Prod17 <= prod17 [21:8];
Prod18 <= prod18 [21:8];
Prod19 <= prod19 [21:8];
Prod20 <= prod20 [21:8];
Prod21 <= prod21 [21:8];
Prod22 <= prod22 [21:8];
Prod23 <= prod23 [21:8];
Prod24 <= prod24 [21:8];
Prod25 <= prod25 [21:8];
Prod26 <= prod26 [21:8];
Prod27 <= prod27 [21:8];
Prod28 <= prod28 [21:8];
Prod29 <= prod29 [21:8];
Prod30 <= prod30 [21:8];
Prod31 <= prod31 [21:8];
Prod32 <= prod32 [21:8];
Prod33 <= prod33 [21:8];
Prod34 <= prod34 [21:8];
Prod35 <= prod35 [21:8];
Prod36 <= prod36 [21:8];
Prod37 <= prod37 [21:8];
Prod38 <= prod38 [21:8];
Prod39 <= prod39 [21:8];
Prod40 <= prod40 [21:8];
Prod41 <= prod41 [21:8];
Prod42 <= prod42 [21:8];
Prod43 <= prod43 [21:8];
```

```

Prod44 <= prod44 [21:8];
Prod45 <= prod45 [21:8];
Prod46 <= prod46 [21:8];
Prod47 <= prod47 [21:8];
Prod48 <= prod48 [21:8];
Prod49 <= prod49 [21:8];
Prod50 <= prod50 [21:8];

add1 <= Prod0 + Prod1 + Prod2 + Prod3;
add1b <= Prod4 + Prod5 + Prod6 + Prod7;
add2 <= Prod8 + Prod9 + Prod10 + Prod11;
add2b <= Prod12 + Prod13 + Prod14 + Prod15;
add3 <= Prod16 + Prod16 + Prod17 + Prod18;
add3b <= Prod19 + Prod20 + Prod21 + Prod22;
add4 <= Prod23 + Prod24 + Prod25 + Prod26;
add4b <= Prod26 + Prod27 + Prod28 + Prod29;
add5 <= Prod30 + Prod31 + Prod32 + Prod33;
add5b <= Prod34 + Prod35 + Prod36 + Prod36;
add6 <= Prod37 + Prod38 + Prod39 + Prod40;
add6b <= Prod41 + Prod42 + Prod43 + Prod44;
add7 <= Prod45 + Prod46 + Prod46 + Prod47;
add7b <= Prod48 + Prod49 + Prod50;

addtotal1 <= add1 + add1b + add2 + add2b;
addtotal2 <= add3 + add3b + add4 + add4b;
addtotal3 <= add5 + add5b + add6 + add6b;
addtotal4 <= add7 + add7b;

addfinal <= addtotal1 + addtotal2 + addtotal3 +addtotal4;

y <= $signed({addtrunc1[16:16], addtrunc1[14:2]}) ;
yunsign <= y*10 + 14'b 10000000000000;
//y = addtrunc1[13:0];

end

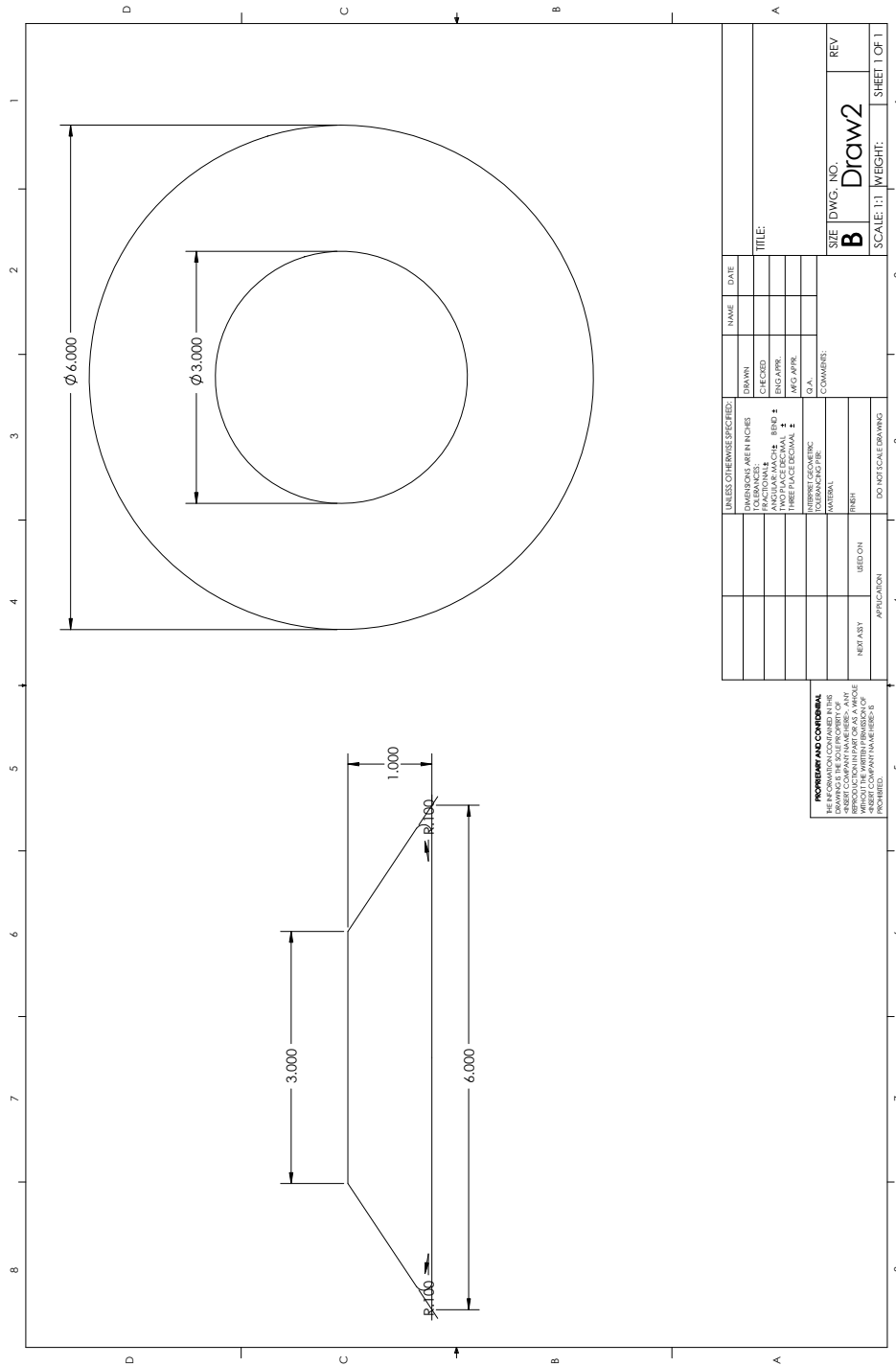
always @(addfinal) begin
    addtrunc1 = addfinal + 17'b 00000000000000010;
end

endmodule

```

Appendix B

Magnetic Design Drawings



SolidWorks Student License
Academic Use Only

Figure B-2: Solidworks drawing of the machined pole pieces used in the improved magnetic system.

Bibliography

- [1] C. Hayes A. Sahakian and B. Yalvac. An inexpensive laboratory module to teach principles of nmr/mri. *Proceedings of the 2005 American Society for Engineering Education Annual Conference & Exposition*, 2005.
- [2] D.M. Cole E. Esparza-Coss. A low-cost mri permanent magnet prototype.
- [3] E. Fukushima and S. Roeder. *Experimental Pulse NMR: A Nuts and Bolts Approach*. Addison-Wesley Publing Company, Inc., 1981.
- [4] Johnson G Hutchison JMS, Edelstein WA. A whole body nmr imaging machine. *J Phys E Sci Instrum*, 13:947– 955, 1980.
- [5] K. Iniewski. *Medical Imaging: Principles, Detectors, and Electronics*. John Wiley and Sons, Inc., 2009.
- [6] M. F. Schlecht J. G. Kassakian and G. C. Verghese. *Principles of Power Electronics*. Addison-Wesley, 1991.
- [7] J. Kirsch and R. Newman. A pulse nmr experiment for an undergraduate physics laboratory.
- [8] M. Thompson R. Venkatesan M. Haacke, R. Brown. *Magnetic Resonance Imaging: Physical Principle and Sequence Design*. John Wiley and Sons, Inc., 1999.
- [9] C.R. Nave. Hyperphysics. <http://hyperphysics.phy-astr.gsu.edu/HBASE/top.html>, 2006.
- [10] J. R. Porter D.C. Spence E. Esparza D.C. Cole S.M. Wright, D.G. Brown and F.R. Huson. A desktop magnetic resonance imaging system. *Magnetic Resonance Materials in Physics, Biology and Medicine*, 13:177–185, January 2002.
- [11] D. Staelin. *6.013 Electromagnetics and Applications*. MIT Copy Technology Centers, 2008.